Electroneutral models for a multidimensional dynamic Poisson-Nernst-Planck system

Zilong Song, Xiulei Cao, and Huaxiong Huang*
Department of Mathematics and Statistics, York University and Fields Institute for Research in Mathematical Sciences, Toronto, Ontario, Canada

(Received 19 June 2018; published 7 September 2018)

The Poisson-Nernst-Planck (PNP) system is a standard model for describing ion transport. In many applications, e.g., ions in biological tissues, the presence of thin boundary layers poses both modeling and computational challenges. In a previous paper, we derived simplified electro-neutral (EN) models in one-dimensional space where the thin boundary layers are replaced by effective boundary conditions. In this paper, we extend our analysis to the multidimensional case where the EN model enjoys even greater advantages. First, it is much cheaper to solve the EN models numerically. Second, EN models are easier to deal with compared with the original PNP system, therefore it is also easier to derive macroscopic models for cellular structures using EN models. The multi-ion case with a general boundary is considered for a variety of boundary conditions including either Dirichlet or flux boundary conditions. Using systematic asymptotic analysis, we derive a variety of effective boundary conditions directly applicable to the EN system for the bulk region. To validate the EN models, numerical computations are carried out for both the EN and original PNP system, including the propagation of action potential for both myelinated and unmyelinated axons. Our results show that solving the EN models is much more efficient than the original PNP system.

DOI: 10.1103/PhysRevE.98.032404

I. INTRODUCTION

Ion transport plays a critical role in normal biological functions, and in many cases, excessive charges accumulate next to cell membranes and form thin boundary layers (BLs). These BLs constantly adapt to the in- and ef-fluxes of ions through pores formed by proteins embedded in cell membranes, affecting membrane potential and therefore cellular functions. When the overall flux is negligible, and these changes in the BLs occur over a timescale shorter than that of the normal biological function, one can approximate the charge accumulation in the BL by an effective capacitor. On the other hand, when the overall flux is not small, ignoring these changes lead to inconsistency in the electro-neutral status of an ionic solution away from these thin layers. In Ref. [1] effective boundary conditions were derived so that BLs do not need to be considered explicitly when the main interest of the investigation is focused on the evolution of the bulk ionic concentration, under the Dirichlet conditions for ions. An extension to other boundary conditions including flux conditions was given in our previous work [2] for the problem in one-dimensional (1D) space.

The Poisson-Nernst-Planck (PNP) system is a mathematical model that describes the ion transport under the influence of both an ionic concentration gradient and an electric field. It is essentially a system coupling diffusion and electrostatics, and the nonlinearity comes from the drift effect of electric field on ions. Such a system and its variants have extensive and successful applications in biological systems, particularly ion channels on cell membranes [3,4]. It has also been applied to many industrial fields, such as semiconductor devices [5] and the detection of poisonous lead by ion-selective electrodes [6].

When applied to the biological systems, the PNP system will possess a small dimensionless parameter. Such a small parameter leads to the presence of BLs near the boundary of the concerned domain, often called Debye or double layer in the literature. For many decades, research efforts have been devoted to BL analysis of the PNP systems. For example, singular perturbation analysis of PNP systems has been carried out for narrow ion channels with a certain geometric structure [7,8]. A geometric singular perturbation approach has been developed to investigate the existence and uniqueness of solutions in a stationary PNP system [9,10] as well as the effects of permanent charge and ion size [11,12]. For a general steady-state case, Wang *et al.* [13] have managed to reduce the asymptotic solutions to a single scalar transcendental equation.

Generally speaking, in BL analysis, the solution of a PNP system consists of two parts: the BL solution near the boundary and the bulk solution in the interior region of the domain. The two solutions are connected by some matching conditions. In 1D cases, some matching or continuity condition has been proposed, e.g., the continuity of an electrochemical potential in Ref. [1]. This has been successfully applied to the study of steady states of 1D systems, showing the existence of multiple steady states with piecewise constant fixed charge [14]. In a previous paper [2], we have conducted a systematic BL study for the 1D dynamical PNP system and derived various effective boundary conditions. We have also managed to bring back high-order contributions into such effective conditions, which are not negligible in most biological applications. However, most practical cases are two- or three-dimensional (2D or 3D), and we will extend the study to the 2D case in this paper (3D is a straightforward

*Corresponding author: hhuang@fields.utoronto.ca

generalization). These conditions replace the BL and have potential applications for deriving macroscopic models [15] for the bulk region in complicated structures. For example, macro-equations are derived in the bulk region for the lens circulation [16,17], by taking into account the fluxes through membranes but ignoring the BL (where the fluxes calculated there might not be accurate).

In addition to BL analysis, many conservative numerical schemes have been developed for PNP systems, such as the finite element method [18], finite-difference scheme [19], and finite volume method [20–22], in one- and higher-dimensional spaces [23,24]. It is well known that one challenge of computation of PNP is how to accurately capture the BL. Since functions vary rapidly in the BL, more mesh points are needed in the BL than in the bulk region to attain certain accuracy [25,26]. This increases the computational cost and/or requires more sophisticated numerical approaches, especially when there are many BLs in a complicated system. One attractive idea is to derive effective conditions at the boundary to avoid the need for resolving the BL, so that computation is needed only for the bulk region. This becomes extremely important in the multidimensional case and is the other motivation of the current work. Our electro-neutral (EN) model with effective boundary conditions can be solved with much less computational power compared to the original PNP system. This will be demonstrated in many numerical examples, in particular the propagation of an action potential along axon.

The rest of the paper is structured as follows. In Sec. II we present the EN theories. First, to illustrate the ideas, we will study the two-ion case with a circular boundary. This is followed by generalizations to multi-ion cases with general boundaries. In Sec. III these effective boundary conditions are validated by several numerical examples. In Sec. IV we study one specific biological application, i.e., the propagation of the action potential along an axon. Our EN model, together with effective interface conditions, is very efficient to capture the propagation of action potential. Finally conclusions and discussion of future directions are given in Sec. V.

II. THE ELECTRO-NEUTRAL THEORIES

In this section, we investigate the 2D (or 3D) dynamical PNP system and derive electro-neutral (EN) systems with various effective boundary conditions. The domain is set to be Ω with boundary $\Gamma = \partial\Omega$. First, to illustrate the main ideas, we will study the two-ion case with valencies ± 1 and with a circular boundary Γ. Then it is easily generalized to multi-ion case with general boundaries.

Now we briefly recall the 2D (or 3D) dynamical PNP system and introduce some assumptions for deriving EN systems. Suppose there are n ion species, and let p_i be the ion concentrations and ψ be the electric potential. In Ω, the dimensional PNP system is given by

$$\begin{aligned} -\epsilon_0\epsilon_r\Delta\psi &= e_0 N_A \sum_{i=1}^{n} z_i p_i, \\ \partial_t p_i &= -\nabla\cdot\mathbf{J}_{p_i} = D_i\nabla\cdot\left(\nabla p_i + \frac{e_0}{k_B T} z_i p_i \nabla\psi\right), \end{aligned} \tag{1}$$

where $i = 1, \ldots, n$. The first equation is the electrostatic Poisson equation for $\psi(\mathbf{x}, t)$ ($\mathbf{x} \in \Omega$), and the second (Nernst-Planck) equation describes the ion transport for each ion species $p_i(\mathbf{x}, t)$ ($i = 1, \ldots, n$). The quantity $\mathbf{J}_{p_i}$ is the associated flux vector for p_i, and D_i is the diffusion constant. The flux consists of two parts: the linear part due to the ionic concentration gradient and the nonlinear part from the drift effect of the electric field. Other parameters are the vacuum permittivity ϵ_0, relative permittivity ϵ_r, elementary charge e_0, Avogadro constant N_A, Boltzmann constant k_B, and absolute temperature T.

In the following, we will consider the dimensionless or normalized version of the above PNP system; see Appendix D for details of a nondimensionalization process. We still adopt the same notations, and the PNP system for dimensionless quantities p_i, ψ in the normalized domain Ω is given by

$$\begin{aligned} -\epsilon^2\Delta\psi &= \sum_{i=1}^{n} z_i p_i, \\ \partial_t p_i &= -\nabla\cdot\mathbf{J}_{p_i} = D_i\nabla\cdot(\nabla p_i + z_i p_i \nabla\psi), \end{aligned} \tag{2}$$

where $i = 1, \ldots, n$, and D_i are some dimensionless diffusion constants. Here $\epsilon \ll 1$ is a dimensionless small parameter and defined by

$$\epsilon = \sqrt{\frac{\epsilon_0\epsilon_r k_B T}{e^2 N_A p_0 L^2}}, \tag{3}$$

where p_0 is some typical ion concentration and L is some typical length of domain. This system is accompanied by some initial conditions for p_i and some suitable boundary conditions for both ψ and p_i. For example, we may propose either a Dirichlet condition or flux condition for each ion species p_i. The initial effect is not considered in this work, and we mainly limit ourselves to the case when the BL is already present or gradually appears.

As in the 1D case [2], we assume that local electro-neutrality (LEN) condition in the bulk region is satisfied, and moreover the near global electro-neutrality (NGEN) condition is satisfied, i.e., there is only at most $O(\epsilon)$ unbalanced charge. The second assumption essentially puts some restriction on the boundary conditions; see Remarks 3 and 4 in later sections. These conditions can be justified in many biological applications, for example, in the neuronal axon [27]. It is then natural to assume in the bulk region all the functions concerned, and their derivatives are $O(1)$:

$$\psi, \nabla\psi, \ldots \sim O(1), \quad p_i, \partial_t p_i, \nabla p_i, \ldots \sim O(1). \tag{4}$$

In the next subsections, we will derive the EN systems and associated effective boundary conditions based on these assumptions.

A. Two-ion case with circular boundary

In this subsection, we investigate the typical case of two ions with valences $z_1 = 1, z_2 = -1$. Suppose that the boundary Γ is a circle with radius $r_0 \sim O(1)$. Polar coordinates (r, θ) will be adopted. We denote the cation and anion as $p_1(\mathbf{x}, t) = p(r, \theta, t)$ and $p_2(\mathbf{x}, t) = n(r, \theta, t)$, and write $\psi(\mathbf{x}, t) = \psi(r, \theta, t)$.

From (2), the original PNP system for p, n, ψ is written as

$$\begin{aligned} -\epsilon^2\left(\frac{\partial^2\psi}{\partial r^2}+\frac{1}{r}\frac{\partial\psi}{\partial r}+\frac{1}{r^2}\frac{\partial^2\psi}{\partial\theta^2}\right) &= p-n,\\ -\partial_t p &= \frac{\partial J_p^r}{\partial r}+\frac{1}{r}\frac{\partial J_p^\theta}{\partial\theta}+\frac{1}{r}J_p^r,\\ -\partial_t n &= \frac{\partial J_n^r}{\partial r}+\frac{1}{r}\frac{\partial J_n^\theta}{\partial\theta}+\frac{1}{r}J_n^r, \end{aligned} \tag{5}$$

where superscripts r, θ denote the normal and circumferential fluxes.

Based on the previous assumptions, we obtain approximately the EN condition $p \approx n$ from the first equation in Eq. (5), and more precisely we write in the bulk region

$$p = n = c + O(\epsilon^2), \quad \psi = \phi + O(\epsilon^2). \tag{6}$$

Thus, the reduced EN system for c and ϕ is

$$\begin{aligned} \partial_t c &= -\nabla\cdot\mathbf{J}_c^+ = \nabla\cdot(\nabla c + c\nabla\phi),\\ \partial_t c &= -\nabla\cdot\mathbf{J}_c^- = \nabla\cdot(\nabla c - c\nabla\phi), \end{aligned} \tag{7}$$

with remainder $O(\epsilon^2)$, and it is equivalent to

$$\partial_t c = \Delta c, \quad \nabla\cdot(c\nabla\phi) = 0. \tag{8}$$

The first equation is the standard diffusion equation for the common concentration c in bulk, and the second is the continuity equation of electric current with effective conductance c. In polar coordinates, (7) can be written as

$$-\partial_t c = \frac{\partial J_c^{r,\pm}}{\partial r}+\frac{1}{r}\frac{\partial J_c^{\theta,\pm}}{\partial\theta}+\frac{1}{r}J_c^{r,\pm}, \tag{9}$$

where $J_c^{r,\pm}$, $J_c^{\theta,\pm}$ are normal and circumferential components of fluxes $\mathbf{J}_c^\pm$. Then the objective is to find two effective boundary conditions for the EN system (8), based on three exact boundary conditions for the PNP system (5). In the following, we present the results for the cases of Dirichlet boundary conditions and flux boundary conditions. The proofs of Propositions 1 and 2 are given in Appendix A.

Proposition 1. Suppose the LEN and NGEN conditions are satisfied, the PNP system (5) is defined in circular domain $r < r_0$, and the Dirichlet boundary conditions are given by

$$\begin{aligned} \psi(r_0,\theta,t) &= \psi_0(\theta,t),\\ p(r_0,\theta,t) &= p_0(\theta,t),\\ n(r_0,\theta,t) &= n_0(\theta,t), \end{aligned} \tag{10}$$

where the subscript 0 denotes quantities at $r = r_0$, then we have the effective boundary conditions for the EN system (8)

$$\begin{aligned} \ln c_0 + \phi_0 - \frac{\sqrt{2}J_{c,0}^{r,+}\epsilon}{(c_0)^{3/2}}(e^{(\psi_0-\phi_0)/2}-1) &= \ln p_0 + \psi_0 + o(\epsilon),\\ \ln c_0 - \phi_0 - \frac{\sqrt{2}J_{c,0}^{r,-}\epsilon}{(c_0)^{3/2}}(e^{(\phi_0-\psi_0)/2}-1) &= \ln n_0 - \psi_0 + o(\epsilon), \end{aligned} \tag{11}$$

where $J_{c,0}^{r,\pm}$ denotes the normal flux $J_c^{r,\pm}$ at $r = r_0$.

Remark 1. The leading-order condition in Eq. (11) is often referred to as the continuity of electro-chemical (EC) potential [1]. The high-order $O(\epsilon)$ correction indicates that if the flux is 0 (e.g., the steady state), EC potential is constant across BL, otherwise the flux modifies the EC potential at next order. For practical implementation, one can use the equivalent boundary conditions for c_0 and ϕ_0:

$$\begin{aligned} c_0 &= \sqrt{p_0 n_0} + \epsilon\frac{n_0^{1/4}-p_0^{1/4}}{\sqrt{2}\sqrt{p_0 n_0}}\left(n_0^{1/4}J_{c,0}^{r,+} - p_0^{1/4}J_{c,0}^{r,-}\right),\\ \phi_0 &= \psi_0 + \frac{1}{2}\ln(p_0/n_0)\\ &\quad + \epsilon\frac{n_0^{1/4}-p_0^{1/4}}{\sqrt{2}n_0 p_0}\left(n_0^{1/4}J_{c,0}^{r,+} + p_0^{1/4}J_{c,0}^{r,-}\right). \end{aligned} \tag{12}$$

The leading order terms are exactly the Dirichlet boundary conditions for c, ϕ in the EN system (8), and to include correction terms one could simplify approximate the fluxes $J_{c,0}^{r,\pm}$ from the previous time step (see Sec. III B).

Proposition 2. Suppose the assumptions are the same as Proposition 1, and the flux boundary conditions for PNP system (5) are given by

$$\begin{aligned} J_p^r(r_0,\theta,t) &= J_{p,0}^r(\theta,t),\\ J_n^r(r_0,\theta,t) &= J_{n,0}^r(\theta,t),\\ \psi(r_0,\theta,t) &= \psi_0(\theta,t), \end{aligned} \tag{13}$$

then we have the effective boundary conditions for the EN system (8):

$$\begin{aligned} J_{c,0}^{r,+} &= J_{p,0}^r + \epsilon\partial_t[\sqrt{2c_0}(e^{\zeta/2}-1)]\\ &\quad - \frac{\epsilon}{r_0^2}\partial_\theta\{\sqrt{2c_0}(e^{\zeta/2}-1)\partial_\theta[\ln c_0 + \phi_0]\} + o(\epsilon),\\ J_{c,0}^{r,-} &= J_{n,0}^r + \epsilon\partial_t[\sqrt{2c_0}(e^{-\zeta/2}-1)]\\ &\quad - \frac{\epsilon}{r_0^2}\partial_\theta\{\sqrt{2c_0}(e^{-\zeta/2}-1)\partial_\theta[\ln c_0 - \phi_0]\} + o(\epsilon), \end{aligned} \tag{14}$$

where $\zeta = \phi_0 - \psi_0$ is the zeta potential, and the subscript 0 denotes quantities at $r = r_0$.

Remark 2. Keeping the $O(\epsilon)$ terms in Eq. (14) is necessary for two reasons. First, in bulk equations (7) we have assumed an $O(\epsilon^2)$ remainder, so it is reasonable and consistent to bring back the $O(\epsilon)$ terms on boundary conditions. Second, neglecting the $O(\epsilon)$ terms is physically incorrect for EN system as the solution would not be unique (e.g., ϕ can differ by a constant). The effective flux conditions incorporate two effects: (1) the ∂_t term accounts for the accumulation of ions in BL, like a capacitor and (2) the ∂_θ term represents the spacial variation along the circumferential boundary. Such terms can be essential in many biological applications, as in the example of the action potential in later sections. For practical implementation, one can do an addition and a subtraction of these two conditions to obtain formulas for fluxes $\partial_r c$ and $c\partial_r\phi$ at the boundary for the system (8). The high-order terms also involve c_0, ϕ_0, and usually an implicit scheme will be used.

Remark 3. In the above proposition, the given fluxes $J_{p,0}^r$, $J_{n,0}^r$ can be either $O(1)$ or $O(\epsilon)$, as long as the NGEN is satisfied. This means when fluxes are $O(1)$, we should impose

some restriction on the fluxes,

$$\int_0^t \int_\Gamma \left(J^r_{p,0} - J^r_{n,0}\right) d\Gamma\, dt = O(\epsilon), \tag{15}$$

which means the total current flowing into the domain is $O(\epsilon)$. In some cases, the flux is not explicitly given but is related to the concentrations and electric potential by some model. For example, in biological applications there is the Hodgkin-Huxley model [27] or GHK flux model [28], and for electrolytes there are Chang-Jaffle boundary conditions [6,29,30]. Suppose the boundary condition is in the form $J^r_{p,0} = f(p_0, \psi_0)$, where f is some given function, then we need to replace $J^r_{p,0}$ by f in Proposition 2 and supplement these effective flux conditions with those conditions in Proposition 1.

B. Multi-ion case with general boundary

In this subsection, we extend the preceding results for two ion species to the general multi-ion species case, and we consider a domain Ω inside a general 2D boundary Γ. We assume that Γ is smooth without singularities and that the curvature is not too large, say, $O(1)$.

We use curvilinear coordinates to represent a region near boundary. The boundary Γ is parametrized by a variable η, and let ξ denote the signed distance (outward means positive) to the boundary. The tangent vector along Γ is defined by

$$\mathbf{g}_\eta = \frac{d\mathbf{s}}{d\eta} = g(\eta)\mathbf{e}_\eta, \tag{16}$$

where $\mathbf{s}(\eta)$ represents the position vector on the boundary. The function $g(\eta)$ is the metric and $g = 1$ if η is suitably chosen as the arc length variable, and $\mathbf{e}_\eta$ is the tangent unit vector. The unit outward normal to the boundary is denoted by $\mathbf{e}_\xi$. Then the curvature $\kappa(\eta)$ on the boundary is defined by

$$\kappa(\eta) = -\frac{1}{g(\eta)} \frac{d\mathbf{e}_\xi}{d\eta} \cdot \mathbf{e}_\eta. \tag{17}$$

We consider the original PNP system (2) with n species of ions. With previous assumptions, we write in the bulk region

$$p_i = c_i + O(\epsilon^2), \quad \psi = \phi + O(\epsilon^2). \tag{18}$$

Then the EN system for bulk region is

$$\partial_t c_i = -\nabla \cdot \mathbf{J}_{c_i} = D_i \nabla \cdot (\nabla c_i + z_i c_i \nabla \phi), \tag{19}$$

where $i = 1, \ldots, n$. Alternatively, by the EN condition $\sum_{i=1}^n z_i c_i = 0$, the above EN system for n unknowns $c_1, \ldots, c_{n-1}, \phi$ can be written as

$$\begin{aligned} &\partial_t c_i = -\nabla \cdot \mathbf{J}_{c_i} = D_i \nabla \cdot (\nabla c_i + z_i c_i \nabla \phi), \\ &\sum_{k=1}^n z_k D_k \nabla \cdot (\nabla c_k + z_k c_k \nabla \phi) = 0, \end{aligned} \tag{20}$$

for $i = 1, \ldots, n-1$ and whenever c_n appears we should replace it by $c_n = -\frac{1}{z_n} \sum_{i=1}^{n-1} z_i c_i$. The last equation in Eq. (20) is roughly the current continuity equation for ϕ, e.g., if $D_i = D_0$ are the same constant, then the last equation for ϕ reduces to $\nabla \cdot (\sigma \nabla \phi) = 0$ with the effective conductance $\sigma = \sum_{k=1}^n z_k^2 c_k$. In the following theorems, we present three cases of boundary conditions and associated effective boundary conditions for EN system (20), and the proofs are given in Appendix A.

Theorem 1. Suppose LEN and NGEN conditions are satisfied, and let (ξ, η) be the local coordinates near the boundary $\Gamma = \partial\Omega$. The boundary Γ is characterized by metric $g(\eta)$ and curvature $\kappa(\eta)$, which are supposed to be $O(1)$. For PNP system (2), the boundary conditions of normal fluxes and electric potential are given by

$$\psi(0, \eta, t) = \psi_0(\eta, t), \quad J^\xi_{p_i}(0, \eta, t) = J^\xi_{p_i,0}(\eta, t), \tag{21}$$

then we have the effective boundary conditions for EN system (20)

$$J^\xi_{c_i,0} = J^\xi_{p_i,0} + \epsilon \partial_t F_{i0} - \epsilon \nabla_\Gamma \cdot (D_i F_{i0} \nabla_\Gamma \mu_{i0}) + o(\epsilon), \tag{22}$$

where $\nabla_\Gamma = \frac{1}{g}\partial_\eta$ in this 2D case, and the subscript 0 denotes quantities on the boundary Γ (i.e., at $\xi = 0$), and

$$\begin{aligned} \mu_{i0} &= \ln c_{i0} + z_i \phi_0, \\ F_{i0} &= F_i(c_{10}, \ldots, c_{n-1,0}, \phi_0 - \psi_0) \\ &= \pm \frac{c_{i0}}{\sqrt{2}} \int_1^{e^{\phi_0 - \psi_0}} \frac{u^{z_i} - 1}{\sqrt{\sum_{k=1}^n c_{k0}(u^{z_k} - 1)}} \frac{du}{u}. \end{aligned} \tag{23}$$

In F_i, the $\pm$ are chosen for the cases $\psi_0 \leqslant \phi_0$ and $\psi_0 \geqslant \phi_0$ respectively, but F_i is well defined around $\phi_0 = \psi_0$, and if F_i can be integrated out, the expressions from the two cases are the same (see Appendix B).

Remark 4. The above theorem is also valid in three dimensions; see the proof in Appendix A (in three dimensions the following Theorems 2 and 3 will not change). In above 2D case, the surface gradient ∇_Γ is a scalar operator, and for the 3D case ∇_Γ will be a vector operator on a surface. The ∇_Γ term is similar to a term in Eq. (2.246) of Ref. [31] under linearization of F_{i0}. In the above effective conditions, the ∂_t term plays a role of a nonlinear capacitor, and the ∇_Γ term accounts for the ion transport in BLs along the boundary. In view of definition (A31), the term F_{i0} accounts for the accumulation of the ith ion in the BL. Only the metric parameter $g(\eta)$ is present, while the curvature does not influence them as long as it is not very large. For the two-ion case with formula (B1), the above conditions reduce to those in Proposition 2. Similar arguments in Remarks 2 and 3 still apply here; particularly, the integrand in Eq. (15) should be replaced by $\sum_{i=1}^n J^\xi_{p_i,0}$. For practical implementation, the conditions of $J^\xi_{c_i,0}$ $(i = 1, \ldots, n-1)$ in Eq. (22) provide flux conditions for $(20)_1$, and the summation $\sum_{i=1}^n z_i J^\xi_{c_i,0}$ gives the flux condition for $(20)_2$.

Theorem 2. Suppose the assumptions are the same as Theorem 1. For the PNP system (2), the Dirichlet boundary conditions on Γ are given by

$$\psi(0, \eta, t) = \psi_0(\eta, t), \quad p_i(0, \eta, t) = p_{i0}(\eta, t), \tag{24}$$

where $i = 1, \ldots, n$, then for the EN system (20) we have the effective boundary conditions

$$\ln c_{i0} + z_i \phi_0 - \frac{\epsilon J^\xi_{c_i,0}}{D_i} f_{i0} = \ln p_{i0} + z_i \psi_0 + o(\epsilon), \tag{25}$$

where $i = 1, \ldots, n$, the subscript 0 denotes quantities at $\xi = 0$, and

$$f_{i0} = f_i(c_{10}, \ldots, c_{n-1,0}, \phi_0 - \psi_0) = \pm \frac{1}{\sqrt{2}c_{i0}} \int_1^{e^{\phi_0-\psi_0}} \frac{u^{-z_i} - 1}{\sqrt{\sum_{k=1}^n c_{k0}(u^{z_k} - 1)}} \frac{du}{u}. \quad (26)$$

Here the $\pm$ are chosen for the cases $\psi_0 \leqslant \phi_0$ and $\psi_0 \geqslant \phi_0$, but f_i is well defined around $\phi_0 = \psi_0$, and if f_i can be integrated out, the expressions from the two cases are the same (see Appendix B).

Similar to Remark 1, the leading order conditions are the continuity of the EC potential. For practical implementation, one would use equivalent explicit Dirichlet conditions for c_{i0} and ϕ_0 like (12). The leading order terms together with EN condition imply

$$\sum_{i=1}^n z_i p_{i0} e^{z_i(\psi_0 - \phi_0)} = 0, \quad (27)$$

from which ϕ_0 is obtained, and then c_{i0} $(i = 1, \ldots, n-1)$ are obtained from (25). These are leading order Dirichlet conditions for the EN system (20). Explicit high-order correction can be obtained by replacing quantities c_{i0} and ϕ_0 in f_i by the above leading order approximations.

Theorem 3. Suppose the assumptions are the same as Theorem 1. For the PNP system (2), the boundary conditions on Γ are given by

$$\gamma \partial_\xi \psi(0, \eta, t) = \tilde{\psi}_0(\eta, t) - \psi(0, \eta, t), \qquad J^\xi_{p_i}(0, \eta, t) = J^\xi_{p_i,0}(\eta, t), \quad (28)$$

where $\gamma \leqslant O(1)$ is a parameter and $\tilde{\psi}_0$ is some given function, then for the EN system (20) we have the same effective flux conditions (22) and (23) as in Theorem 1 except that $\psi_0 \equiv \psi(0, \eta, t)$ is determined by

$$\psi_0 - \tilde{\psi}_0 = \pm \frac{\gamma}{\epsilon} \sqrt{2 \sum_{i=1}^n c_{i0}(e^{z_i(\phi_0 - \psi_0)} - 1)}, \quad (29)$$

where $\pm$ are chosen for the cases $\psi_0 \leqslant \phi_0$ and $\psi_0 \geqslant \phi_0$, but the right-hand side is well defined near $\psi_0 = \phi_0$ (see Appendix B).

As the above Robin-type boundary condition often appears in modeling cell membranes, here we briefly mention an example relevant to macroscopic models for cellular structures. Suppose ψ and $\tilde{\psi}$ denote the electric potential inside and outside a cell, and on the tissue scale they are almost a constant ϕ_0 and $\tilde{\phi}_0$ (say, averaged quantities). But they are not constant in the BL near a membrane and are connected by condition (28) on a membrane with $\gamma = \epsilon^2/C_m$ where C_m is some dimensionless membrane capacitance [cf. (45) in Sec. IV]. The average of each ion concentration in the cell may be defined as

$$\bar{p}_i \equiv \frac{1}{V_{\text{cell}}} \int_{V_{\text{cell}}} p_i \, dx = \frac{1}{V_{\text{cell}}} \int_{V_{\text{cell}}} c_i \, dx + \frac{1}{V_{\text{cell}}} \int_{V_{\text{BL}}} p_i - c_i \, dx = c_{i0} + \frac{S_m}{V_{\text{cell}}} \epsilon F_{i0}(c_{10}, \ldots, c_{n-1,0}, \phi_0 - \psi_0), \quad (30)$$

where V_{BL} is some region containing the BL, F_{i0} is in Eqs. (23) or (A31), S_m is the surface area of a cell, c_i in a cell is also considered a constant c_{i0} on the tissue scale, and ψ_0 is determined by (29). As estimated in Remark 10 of Ref. [2], we have $O(\epsilon) \ll \gamma < O(1)$, and hence variation $\phi_0 - \psi_0$ is small as in (A43). Then we can simplify (29) and (30) based on small $\phi_0 - \psi_0$. It is easy to show from (A31) and (29) that

$$z_i F_{i0} = \frac{z_i^2 c_{i0}}{\sqrt{\sum_{k=1}^n z_k^2 c_{k0}}}(\phi_0 - \psi_0),$$

$$\frac{\gamma}{\epsilon} \sqrt{\sum_{k=1}^n z_k^2 c_{k0}(\phi_0 - \psi_0)} = \psi_0 - \tilde{\psi}_0 \approx \phi_0 - \tilde{\phi}_0, \quad (31)$$

and thus F_{i0} can be expressed by averaged quantities $c_{i0}, \phi_0, \tilde{\phi}_0$. By a summation, we see that

$$\sum_{i=1}^n z_i \bar{p}_i = \frac{S_m}{V_{\text{cell}}} \epsilon \sum_{i=1}^n z_i F_{i0} = \frac{S_m}{V_{\text{cell}}} \frac{\epsilon^2}{\gamma}(\phi_0 - \tilde{\phi}_0) = \frac{S_m}{V_{\text{cell}}} C_m(\phi_0 - \tilde{\phi}_0). \quad (32)$$

This means that the averaged quantities $\bar{p}_i$ on a whole cell including BLs do not satisfy electro-neutrality exactly but are approximated by a linear capacitor. This provides one explanation that some works [31,32] in the literature can use a capacitor to model the BL effect in macroscopic models. More details and application to specific situations will be left as future study.

III. NUMERICAL EXAMPLES

In this section, we present some numerical examples to verify the previous effective boundary conditions and to show the accuracy of the EN system.

A. A steady-state problem

As a first example to verify the previous effective conditions, we study a steady-state problem [1,2], since it can be solved analytically for the EN system. We consider an annulus domain Ω, which is defined by $1 \leqslant r \leqslant 2$ in polar coordinates (r, θ). We consider a 2D steady-state case for two ions $p(r, \theta), n(r, \theta)$ with valencies $z_1 = 1, z_2 = -1$. The boundary conditions in (r, θ) coordinates are

$$p(1, \theta) = n(1, \theta) = 1, \quad \psi(1, \theta) = 0, \qquad p(2, \theta) = 1, \quad J^r_n(2, \theta) = 0, \quad \psi(2, \theta) = -V. \quad (33)$$

Due to symmetry, the original PNP system (5) reduces to a 1D problem

$$-\epsilon^2\left(\frac{d^2\psi}{dr^2} + \frac{1}{r}\frac{d\psi}{dr}\right) = p - n, \qquad r\left(\frac{dp}{dr} + p\frac{d\psi}{dr}\right) = -j, \qquad \frac{dn}{\partial r} - n\frac{d\psi}{\partial r} = 0, \quad (34)$$

TABLE I. Comparison of flux j with fixed $V = 1$ and different ϵ, where "Leading" and "Present" are from formulas (37) and (38), and "PNP" is obtained by solving the dynamic PNP system.

ϵ	0.1	0.05	0.01
Leading	1.1353	1.1353	1.1353
Present	1.1687	1.1519	1.1386
PNP	1.1718	1.1527	1.1387

where j is some flux constant. The aim is to determine the current-voltage j-V relation. Hereafter, the argument θ in functions will be omitted. Since it is electro-neutral at $r = 1$, there is only a BL near the outer boundary $r = 2$. The EN system (9) is

$$\frac{dc}{dr} + c\frac{d\phi}{dr} = \frac{-j}{r},$$
$$\frac{dc}{dr} - c\frac{d\phi}{dr} = 0. \tag{35}$$

With boundary condition $c(1) = 1, \phi(1) = 0$, the 1D analytical solution can be obtained:

$$c(r) = 1 - \frac{j}{2}\ln(r), \quad \phi(r) = \ln(c(r)). \tag{36}$$

By continuity of electro-chemical potential at $r = 2$ [see leading order of (11)], we get

$$j = \frac{2(1 - e^{-V/2})}{\ln 2}. \tag{37}$$

The present effective condition (11) implies

$$2\ln\left(1 - \frac{j}{2}\ln 2\right) - 2\epsilon j\left[\frac{\sqrt{2}e^{-V/2}}{(2 - j\ln 2)^2} - \frac{1}{(2 - j\ln 2)^{3/2}}\right] = -V, \tag{38}$$

where an $O(\epsilon)$ correction is present.

In the numerical verification, we use the dynamic system (5) with boundary conditions (33) and the following initial conditions at $t = 0$:

$$p(r, \theta, 0) = 1, \quad n(r, \theta, 0) = 1. \tag{39}$$

The solution tends to the steady-state solution of (33) and (34), and the flux j near the steady state can be found. A finite-volume method with refined mesh near the outer boundary $r = 2$ is adopted in the numerical simulation, since we require more accuracy for flux j. The flux j at time $t = 20$ is almost a constant and used as the exact value. With $V = 1$ and $\epsilon = 0.1, 0.05, 0.01$, we give the results of flux j using leading order condition (37) and the present condition (38) in Table I. It can be seen that the present effective condition produces better results and the $O(\epsilon)$ term is correct. Figure 1 shows the good agreement in the bulk region between EN solution (36) with flux in (38) and the numerical solution at $t = 20$ with $\epsilon = 0.05$. In order to show the error of solution with respect to small parameter ϵ, Table II compares the maximum errors of $c(r)$ and $\phi(r)$ in Eq. (36), in the bulk region [1,1.5] with different ϵ.

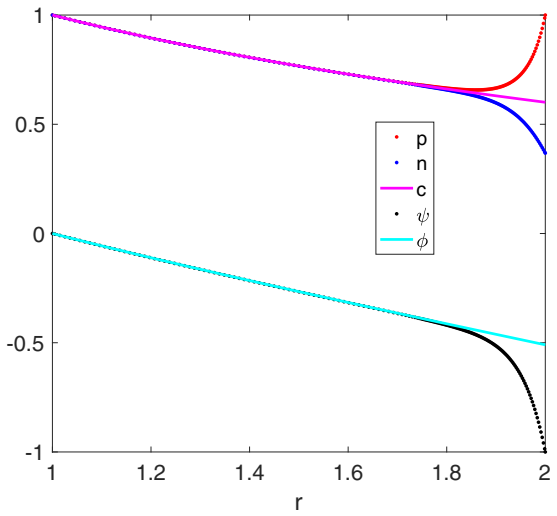

FIG. 1. Comparison between analytic bulk solution with numerical solution at $t = 20$, with $\epsilon = 0.05$. Dots represent the exact solutions of p, n, ψ, and solid lines are the approximate solutions of c, ϕ.

B. A dynamic problem with Dirichlet conditions

Now we consider the circular domain Ω defined by $r \leqslant 1$ and study a dynamic two-ion case with Dirichlet boundary conditions. The original PNP system for p, n, ψ is given by (5), and the boundary conditions are adopted as

$$\psi(1, \theta, t) = 0, \quad p(1, \theta, t) = 1 + t\sin(|\theta|/2),$$
$$n(1, \theta, t) = 1 + t\cos(|\theta|/2), \quad -\pi < \theta \leqslant \pi. \tag{40}$$

In this example, both p and n increase from 1 as time evolves, but the increased magnitudes are different between p and n for fixed θ, and therefore the BL will gradually appear. We take $\epsilon = 0.05$ as an illustration, and the finite element method with refined mesh near boundary $r = 1$ is used to solve this PNP system.

In this example, the EN system in Eq. (8) is solved with effective conditions in Eq. (12) in Remark 1. More precisely, the finite element method (without refined mesh near boundary) is also used in the simulation. We conduct two implementations: (1) with leading order boundary conditions,

$$c(1, \theta, t) = \sqrt{p(1, \theta, t)n(1, \theta, t)},$$
$$\phi(1, \theta, t) = \tfrac{1}{2}\ln(p(1, \theta, t)/n(1, \theta, t)), \tag{41}$$

TABLE II. Comparison of maximum errors of $c(r)$ and $\phi(r)$ in the bulk region $r \in [1, 1.5]$ with different ϵ, where p and n are from dynamic PNP system, and c and ϕ are from (36) with associated flux j in Table I.

ϵ	0.1	0.05	0.01
PNP $\lvert p - n\rvert$	4.8232×10^{-3}	7.3240×10^{-4}	3.1258×10^{-5}
$\lvert c - p\rvert$	2.8585×10^{-3}	1.4192×10^{-3}	5.6801×10^{-4}
$\lvert\psi - \phi\rvert$	5.2579×10^{-3}	1.8024×10^{-3}	5.8205×10^{-4}

TABLE III. Maximum error in concentration $c(x,t)$ and potential $\phi(x,t)$ in some bulk region $r \in [0, 0.5]$ and $t = 0.5$, using leading order condition (41) and present condition (12).

	$\lvert c-p\rvert$	$\lvert\phi-\psi\rvert$
Leading	4.6304×10^{-4}	2.7890×10^{-4}
Present	3.0312×10^{-5}	1.3641×10^{-4}
PNP $\lvert p-n\rvert$	3.3183×10^{-5}	–

and (2) the high-order boundary conditions (12) with a $O(\epsilon)$ term, where an explicit method is used to treat the fluxes $J_{c,0}^{r,\pm}$ (here at $r = 1$) by the estimate from previous time step.

By using the numerical results of $p(x,t)$ and $\psi(x,t)$ of the original system as a reference solution, Table III gives the maximum errors of $c(x,t)$ and $\phi(x,t)$ in some bulk region $r \in [0, 0.5]$ at $t = 0.5$. The results indicate that the accuracy is very good with the effective boundary conditions. Figure 2 shows the comparison between $p(r,\theta,t)$ from the PNP system and $c(r,\theta,t)$ from the EN model, and Fig. 3 shows the comparison between $\psi(r,\theta,t)$ from the PNP system and $\phi(r,\theta,t)$ from the EN model with boundary condition (12) at $t = 0.5$. They show that the approximate solutions $c(x,t)$ and $\phi(x,t)$ agree very well with exact solutions. Furthermore,

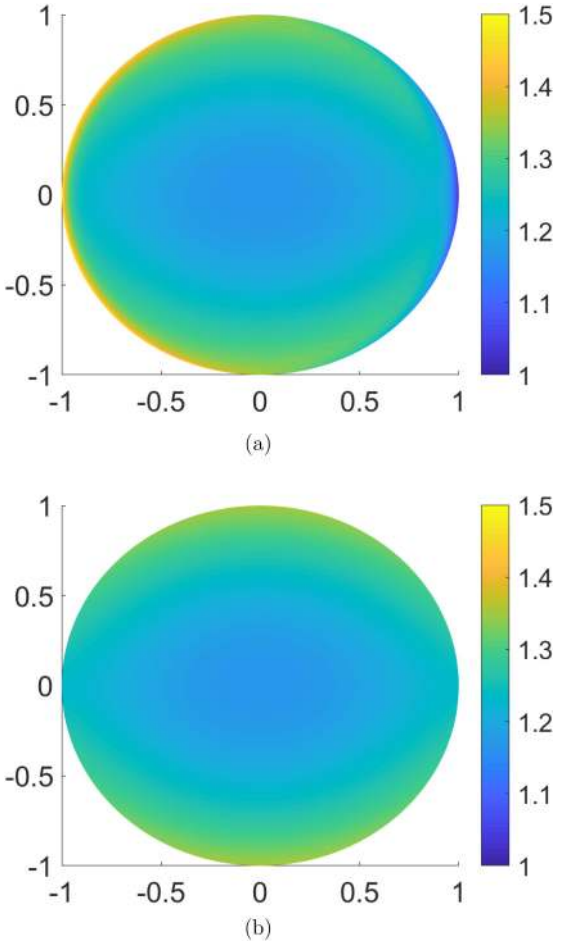

FIG. 2. Comparison of concentrations: (a) $p(r,\theta,t)$ from the PNP system, (b) $c(r,\theta,t)$ from the EN model with present condition (12) at $t = 0.5$.

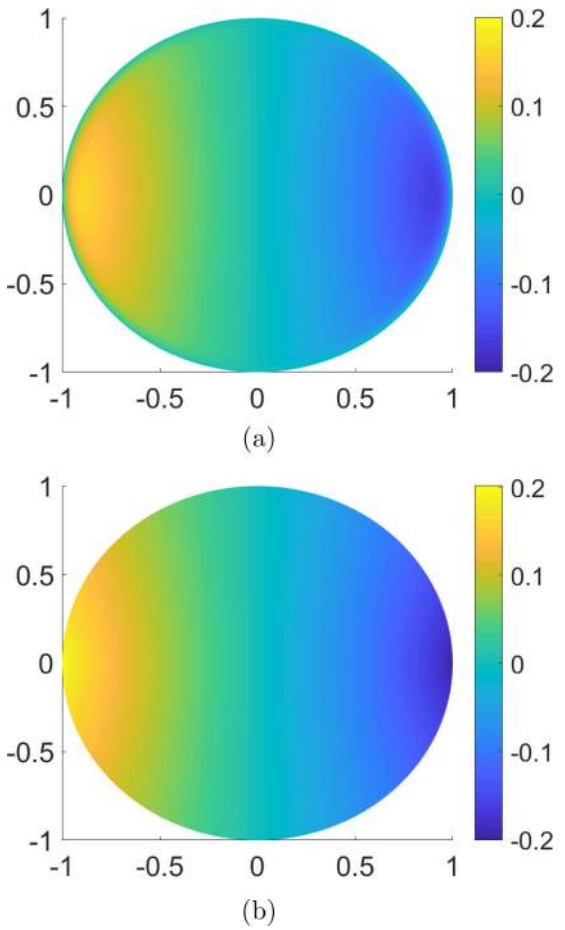

FIG. 3. Comparison of electric potentials: (a) $\psi(r,\theta,t)$ from the PNP system, (b) $\phi(r,\theta,t)$ from the EN model with present condition (12) at $t = 0.5$.

the EN system allows for relatively large mesh and time step sizes, and as a result the computational time is greatly reduced. For instance, it takes roughly 4.8 h to compute the original PNP system up to $t = 0.5$ while it takes only 2 min for the EN system on the same computer (processor: 4 GHz, i76700K; memory: 32 GB).

C. A dynamic problem with flux conditions

As a second dynamic example, we study the two-ion case in circular domain Ω with flux conditions. More precisely, we propose at $r = 1$,

$$\psi(1,\theta,t) = 0, \quad J_p^r(1,\theta,t) = 4\epsilon \sin(\theta),$$
$$J_n^r(1,\theta,t) = 2\epsilon \cos(\theta), \quad -\pi < \theta \leqslant \pi, \tag{42}$$

where $\epsilon = 0.05$ as in the previous example. In this example, the integral of J_p^r or J_n^r over the entire boundary (θ from $-\pi$ to π) will be 0, and so the NGEN condition is automatically satisfied.

In the simulation, a finite element method with refined mesh (as in previous example) is used for the original system (5,42). A uniform mesh is used for EN system (8) together with effective boundary conditions from (14) by an addition and subtraction. For boundary condition (14), a linearized implicit scheme is used to treat the ∂_t term, while an

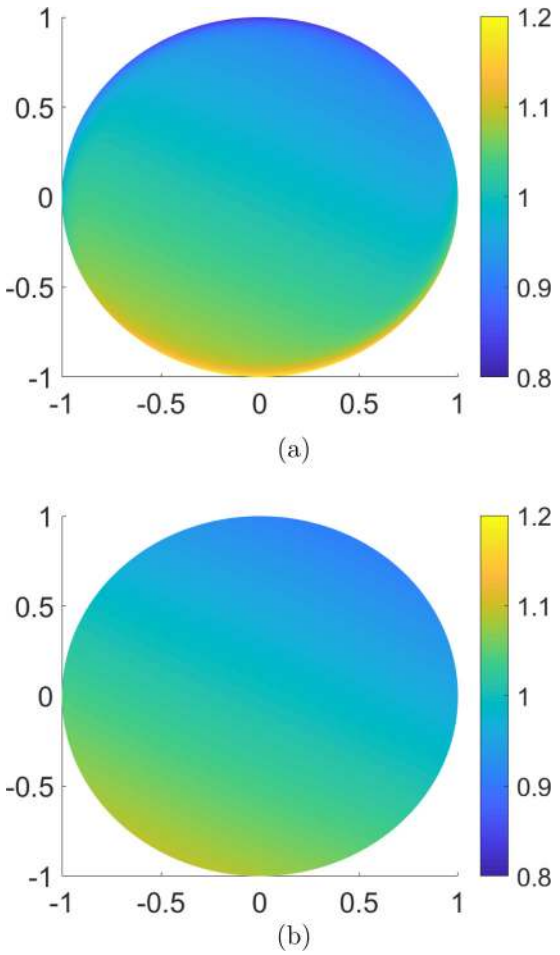

FIG. 4. Comparison of concentrations: (a) $p(r, \theta, t)$ from the PNP system, (b) $c(r, \theta, t)$ from the EN model with present condition (12) at $t = 0.5$.

explicit scheme is used to treat the ∂_θ term. Figure 4 shows the comparison between $p(r, \theta, t)$ from the PNP system and $c(r, \theta, t)$ from the EN model, and Fig. 5 shows the comparison between $\psi(r, \theta, t)$ from the PNP system and $\phi(r, \theta, t)$ from the EN model at $t = 0.5$, which is almost at steady state. They show that the approximate solutions $c(x, t)$ and $\phi(x, t)$ agree very well with exact solutions. The maximum errors of c, ϕ for some bulk region $r \in [0, 0.5]$ at $t = 0.5$ are, respectively, 4.2×10^{-5} and 0.017. Again, the EN system allows for relatively large mesh and time step sizes, and hence the computational time is greatly reduced, i.e., about 4.4 h for the original PNP and 17 min for the EN system on the same computer (processor: 4 GHz, i76700K; memory: 32 GB).

IV. EN MODEL FOR ACTION POTENTIAL PROPAGATION

As a concrete example, we consider the problem of propagation of an action potential along a neuronal axon. This problem was first investigated in Ref. [33] by a cable model. Later many works have simulated it in many cases [34,35] and have attempted to recover the cable model based on the PNP system and other assumptions [36–38]. We refer to the book [39] for a good summary of a cable model. In this section, we first formulate the problem by using a PNP system and

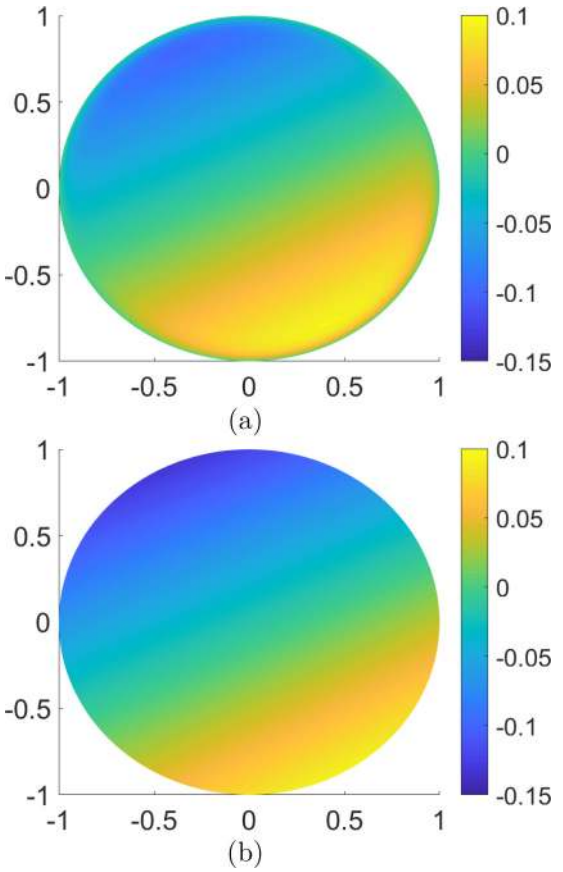

FIG. 5. Comparison of electric potentials: (a) $\psi(r, \theta, t)$ from the PNP system, (b) $\phi(r, \theta, t)$ from the EN model with present condition (12) at $t = 0.5$.

then derive an EN model. Then we present the simulations based on the PNP system and the EN model to show the effectiveness of the EN model.

A. The PNP formulation

Here we follow the formulation based on a PNP system in Ref. [35]. Due to symmetry of the axon, the problem is treated as a 2D problem. In Cartesian coordinates (see Fig. 6), the domain Ω is given by $(x, y) \in [0, L_1] \times [0, L_2]$, where the y direction is normal to the membrane. The membrane is the middle line $y = L_2/2$, the lower region Ω_I is the intracellular space, and the upper region Ω_E is the extracellular space. Only three basic ions (sometimes called bioions) Na^+, K^+, Cl^- are

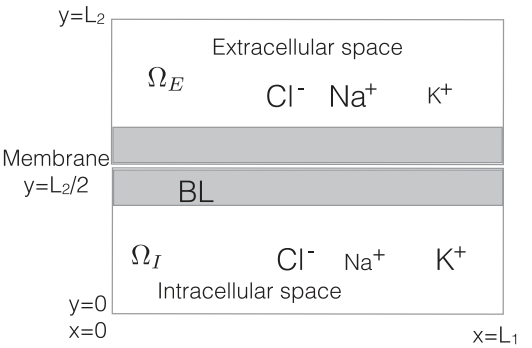

FIG. 6. Sketch of the domain Ω.

considered (the fixed negative charge in Ω_I is incorporated into Cl^- ion as approximation), and the LEN condition in the bulk region is valid in this biological application.

Now we present the system in dimensionless form, and the nondimensionalization process is provided in Appendix D. Let p_i $(i = 1, 2, 3)$ denote ion concentrations of Na^+, K^+, Cl^-, with valences $z_1 = z_2 = 1, z_3 = -1$. By setting $L_2 = 1$, the dimensionless domains become $\Omega_I = [0, L_1] \times [0, 1/2)$ and $\Omega_E = [0, L_1] \times (1/2, 1]$. The final dimensionless PNP system is given by (2) with $n = 3$ in domains Ω_I and Ω_E, with parameter ϵ defined in Appendix D.

The membrane at $y = 1/2$ is described by the Hodgkin-Huxley model [27], in order to simulate an action potential for a neuronal axon. The interface conditions at $y = 1/2$ for the normal flux $J^y_{p_i}$ along the y direction are given by

$$z_i J^y_{p_i}\big|_{y=\frac{1}{2}\pm} = G_{p_i}\left(\psi_I - \psi_E - \frac{1}{z_i}\ln\frac{p_{iE}}{p_{iI}}\right), \tag{43}$$

where G_{p_i} is the dimensionless conductance for ion p_i and possibly depends on variable x (e.g., a myelinated axon). Hereafter, subscripts I and E denote the values or limit values at the membrane $y = 1/2$ from the intracellular and extracellular regions, respectively. Then $V_m = \psi_I - \psi_E$ is defined as the membrane potential. For the part of the axon without a myelin sheath, the conductances G_{p_i} depend on the membrane potential V_m. Following Refs. [2,35], we set

$$\begin{aligned} G_{p_1} &\equiv G_{\mathrm{Na}} = \bar{G}_{\mathrm{Na}} m^3 h + G_{\mathrm{Na,leak}}, \\ G_{p_2} &\equiv G_{\mathrm{K}} = \bar{G}_{\mathrm{K}} n^4 + G_{\mathrm{K,leak}}, \\ G_{p_3} &\equiv G_{\mathrm{Cl}} = 0, \end{aligned} \tag{44}$$

where $\bar{G}_{\mathrm{Na}}, \bar{G}_{\mathrm{K}}, G_{\mathrm{Na,leak}}, G_{\mathrm{K,leak}}$ are some constant given in Appendix C, and n, m, h (associated with potassium channel activation, sodium channel activation, and sodium channel inactivation) depend on V_m and are governed by a dynamic system in Appendix D.

Suppose the membrane has a small thickness, and the electric potential is linear inside the membrane. The associated interface conditions for ψ are given by

$$\epsilon^2 \partial_y \psi\big|_{y=\frac{1}{2}\pm} = C_m(\psi_E - \psi_I), \tag{45}$$

where C_m is the dimensionless capacitance of membrane (defined in Appendix D). All data and specific values of dimensionless quantities for the neuronal axon are presented in Appendix C.

We use typical bulk concentrations as the initial values (see Appendix C) at $t = 0$, then we have

$$\begin{aligned} &p_1(x, y, 0) = 1, \\ &p_2(x, y, 0) = 0.04, \\ &p_3(x, y, 0) = 1.04, \quad \text{in } \Omega_E, \end{aligned} \tag{46}$$

and

$$\begin{aligned} &p_1(x, y, 0) = 0.12, \\ &p_2(x, y, 0) = 1.25, \\ &p_3(x, y, 0) = 1.37, \quad \text{in } \Omega_I. \end{aligned} \tag{47}$$

For the boundary conditions, we adopt Dirichlet conditions on the top boundary (cf. Fig. 6):

$$\begin{aligned} &\psi(x, 1, t) = 0, \quad p_1(x, 1, t) = 1, \\ &p_2(x, 1, t) = 0.04, \quad p_3(x, 1, t) = 1.04, \end{aligned} \tag{48}$$

and zero-flux conditions on other boundaries:

$$\begin{aligned} &\frac{\partial \psi}{\partial y}(x, 0, t) = 0, \quad J^y_{p_i}(x, 0, t) = 0, \\ &\frac{\partial \psi}{\partial x}(0, y, t) = 0, \quad J^x_{p_i}(0, y, t) = 0, \\ &\frac{\partial \psi}{\partial x}(L_1, y, t) = 0, \quad J^x_{p_i}(L_1, y, t) = 0, \end{aligned} \tag{49}$$

where $i = 1, 2, 3$.

B. The EN model with effective flux conditions

By (20), the EN equations for c_1, c_2, ϕ are given by

$$\begin{aligned} &\partial_t c_i = -\nabla \cdot \mathbf{J}_{c_i} = D_i \nabla \cdot (\nabla c_i + z_i c_i \nabla \phi), \\ &\sum_{k=1}^{3} z_k D_k \nabla \cdot (\nabla c_k + z_k c_k \nabla \phi) = 0, \end{aligned} \tag{50}$$

where $i = 1, 2$, $z_1 = z_2 = 1$, $z_3 = -1$, and $c_3 = c_1 + c_2$. The outer boundary $\partial\Omega$ lies in the bulk region, so associated boundary conditions are easily derived from (48) and (49), and we have

$$\begin{aligned} &\phi(x, 1, t) = 0, \quad c_1(x, 1, t) = 1, \quad c_2(x, 1, t) = 0.04, \\ &J^y_{c_k}(x, 0, t) = 0, \quad J^x_{c_k}(0, y, t) = 0, \quad J^x_{c_k}(L_1, y, t) = 0, \end{aligned} \tag{51}$$

where $k = 1, 2, 3$.

As illustrated in Fig. 6, there are BLs at two sides of a membrane. Then we need to propose approximate jump conditions at the middle interface for bulk quantities $c_{iI}, \phi_I, c_{iE}, \phi_E$ $(i = 1, 2)$, where subscripts I, E indicate the limit values at interface $y = 1/2$ from intracellular (lower) and extracellular (upper) regions. Based on previous results in Theorems 1 and 2, we first note that $\eta = x, \xi = \pm(y - 1/2)$, $g = 1$ in the theorems and obtain the following 12 conditions:

$$\begin{aligned} &G_{p_i}\left(\psi_I - \psi_E - \frac{1}{z_i}\ln\frac{p_{iE}}{p_{iI}}\right) \\ &\quad = z_i\left[J^y_{c_i,E} + \epsilon\partial_t F_{iE} - \epsilon D_i \partial_x (F_{iE}\partial_x \mu_{iE})\right], \\ &G_{p_i}\left(\psi_I - \psi_E - \frac{1}{z_i}\ln\frac{p_{iE}}{p_{iI}}\right) \\ &\quad = z_i\left[J^y_{c_i,I} - \epsilon\partial_t F_{iI} + \epsilon D_i \partial_x (F_{iI}\partial_x \mu_{iI})\right], \\ &\ln c_{iE} + z_i\phi_E + \frac{\epsilon J^y_{c_i,E}}{D_i} f_{iE} = \ln p_{iE} + z_i\psi_E, \\ &\ln c_{iI} + z_i\phi_I - \frac{\epsilon J^y_{c_i,I}}{D_i} f_{iI} = \ln p_{iI} + z_i\psi_I, \end{aligned} \tag{52}$$

where $i = 1, 2, 3$, $c_{3I} = c_{1I} + c_{2I}$, $c_{3E} = c_{1E} + c_{2E}$, and we have defined

$$\begin{aligned} \mu_{is} &= \ln c_{is} + z_i\phi_s, \\ F_{is} &= F_i(c_{1s}, c_{2s}, \phi_s - \psi_s), \\ f_{is} &= f_i(c_{1s}, c_{2s}, \phi_s - \psi_s), \quad s = I, E, \end{aligned} \tag{53}$$

where F_i and f_i are given by (B3) and (B6). From Theorem 3, (45), and (B8), we get

$$C_m(\psi_E-\psi_I)=\epsilon\sqrt{2c_{3E}}(e^{(\phi_E-\psi_E)/2}-e^{(\psi_E-\phi_E)/2}),$$
$$C_m(\psi_E-\psi_I)=-\epsilon\sqrt{2c_{3I}}(e^{(\phi_I-\psi_I)/2}-e^{(\psi_I-\phi_I)/2}). \quad (54)$$

From the definition (44) and the data in Appendix C, the conductances are small, i.e., $G_{p_i}\leqslant O(\epsilon)$. Then one can simplify the conditions in Eq. (52) by neglecting higher order $O(\epsilon^2)$ terms, and we obtain the effective flux conditions at the interface:

$$z_i J^y_{c_i,E}=G_{p_i}\left(\phi_I-\phi_E-\frac{1}{z_i}\ln\frac{c_{iE}}{c_{iI}}\right)$$
$$-z_i\epsilon\partial_t F_{iE}+\epsilon D_i z_i\partial_x(F_{iE}\partial_x\mu_{iE}),$$
$$z_i J^y_{c_i,I}=G_{p_i}\left(\phi_I-\phi_E-\frac{1}{z_i}\ln\frac{c_{iE}}{c_{iI}}\right)$$
$$+z_i\epsilon\partial_t F_{iI}-\epsilon D_i z_i\partial_x(F_{iI}\partial_x\mu_{iI}), \quad (55)$$

The ∂_t terms account for the ion accumulation in a BL like a nonlinear capacitor [2], and the ∂_x terms account for the spacial variations along boundary. To summarize, the final EN model consists of (50) and (51) and interface conditions (54) and (55).

Remark 5. By linearization according to small $\phi_I-\psi_I$ and $\phi_E-\psi_E$, we get from (53), (B3), and (54) that

$$\epsilon z_i F_{iI}\approx C_m\lambda_{iI}V_m,$$
$$V_m=\psi_I-\psi_E\approx\phi_I-\phi_E, \quad (56)$$

where

$$\lambda_{iI}=\frac{c_{iI}}{\sum_{k=1}^3 c_{kI}}. \quad (57)$$

Summation of fluxes in Eq. (55) implies

$$\sum_{i=1}^3 z_i J^y_{c_i,I}-\sum_{i=1}^3 G_{p_i}\left(\phi_I-\phi_E-\frac{1}{z_i}\ln\frac{c_{iE}}{c_{iI}}\right)$$
$$\approx C_m\partial_t V_m-C_m\sum_{i=1}^3 D_i\partial_x(\lambda_{iI}V_m\partial_x\mu_{iI}). \quad (58)$$

Physically, the first term is the current from bulk region, the second term is the Hodgkin-Huxley flux model (with bulk quantities), and the right-hand side represents a capacitor and spacial variation along membrane. One can further recover the classic cable model by adopting suitable scaling for variable x, which is left for future study.

C. Numerical simulation

In this subsection, we present numerical results using both the original PNP system and the present EN model. The computation is divided into two steps: first, we generate a resting state, and, second, we simulate the propagation of the action potential. We will study two cases: axons with and without myelin sheath.

First, we study the unmyelinated axon. The length of an axon is much larger than the typical scale of a cell [35,40],

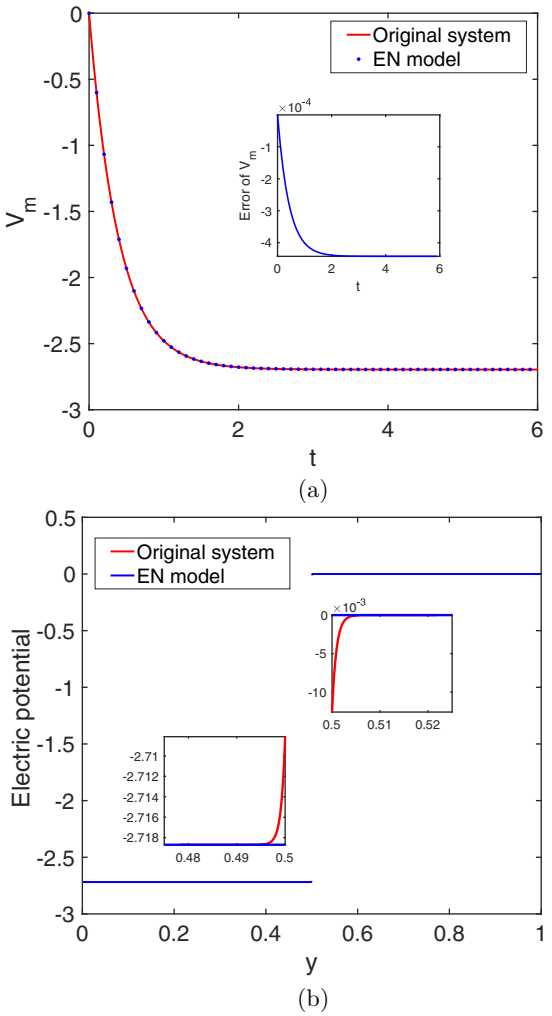

FIG. 7. Numerical results of original system (red) and electroneutral (EN) model (blue) to generate the resting state: (a) dynamics of membrane potential V_m; (b) distribution of electric potential at $t=6$.

and the domain is set to be $\Omega=[0,2000]\times[0,1]$. In step 1, to generate a resting state, we use the conductances in Eq. (44) with equilibrium values for n,m,h given in Eq. (D9). In the computation, we use a 1D code for the y direction, since the problem is uniform in x. For the original model, the finite element method with a nonuniform fixed mesh is adopted, where mesh size varies from 1.6×10^{-4} near the BL to 3.3×10^{-2} in the bulk. A uniform mesh with mesh size 3.3×10^{-2} is adopted in the EN model. The flux of sodium ion $J^y_{p_1}$ is negative, i.e., from Ω_E to Ω_I, while the flux of potassium ion $J^y_{p_2}$ is positive. After a certain period, e.g., at $t=6$, the net flux across the membrane tends to 0, i.e., $J^y_{p_1}+J^y_{p_2}|_{y=1/2}=0$, which is set as the resting state. Figure 7(a) shows the dynamics of membrane potential $V_m=\psi_I-\psi_E$ for both the original model and the new EN model, and the two solutions agree very well with each other (error is shown in the figure). Figure 7(b) shows the distributions of electric potential ψ for the original system and ϕ for the EN model, at resting state $t=6$. They agree very well in the domain except the BL. The resting potential is

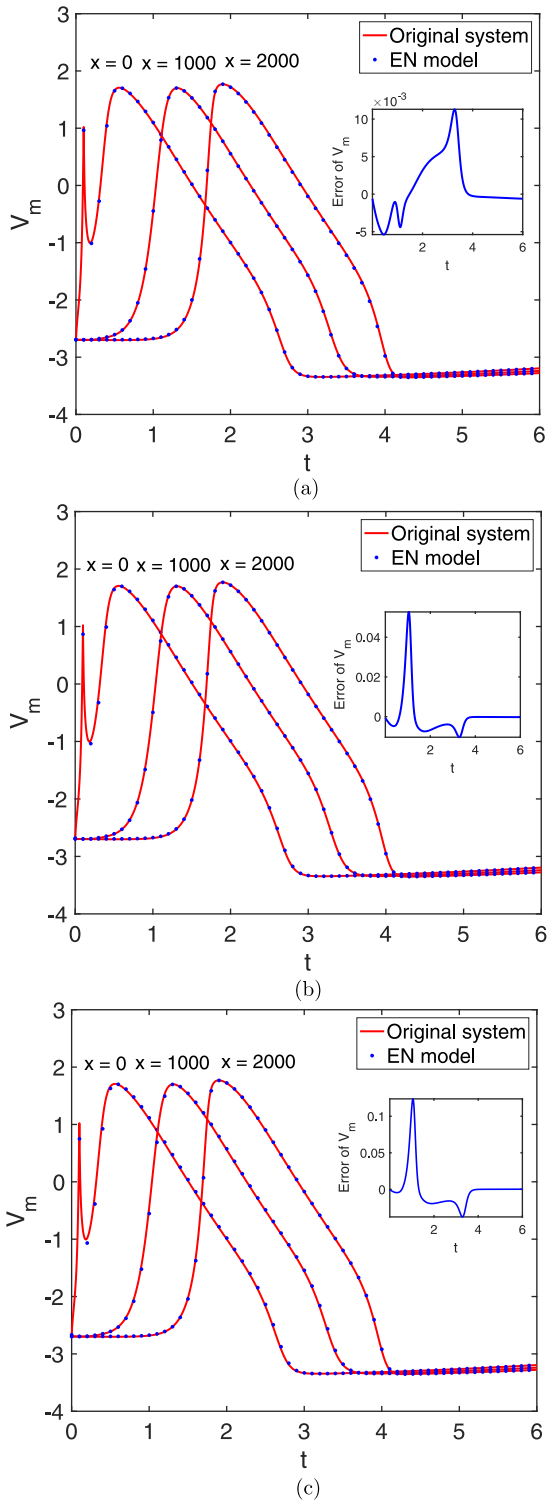

FIG. 8. Numerical results of original system with $\Delta t = 10^{-4}$ and EN model with three different time step sizes: (a) $\Delta t = 10^{-4}$, (b) $\Delta t = 5 \times 10^{-4}$, (c) $\Delta t = 10^{-3}$.

calculated as

$$V_m|_{t=6} = \psi_I - \psi_E|_{t=6} \approx -2.7,$$
$$V_r = \frac{k_B T}{e_0}(\psi_I - \psi_E)|_{t=6} \approx -65\,\text{mV}. \quad (59)$$

TABLE IV. Comparison of computation time between the original system and EN model, and the maximum error for membrane potential V_m in the EN model.

	Original system $\Delta t = 10^{-4}$	EN model, $\Delta t = 10^{-4}$	EN model, $\Delta t = 5 \times 10^{-4}$	EN model, $\Delta t = 10^{-3}$
Error	–	0.01	0.05	0.12
Time	56 h	20 h	3 h	1.9 h

In step 2, to simulate the propagation of action potential [35], we use the conductances in Eq. (44), where n, m, h depend on membrane potential V_m and their dynamics are given in Appendix D. To initiate the action potential near $x = 0$ on the membrane, we increase the conductance of $G_{p_1}(x)$ by modifying $\bar{G}_{Na}$ (to the value 0.6) in the interval $x \in [0, 60]$ for the time period $0 < t < 0.1$. This allows an extra influx of sodium ions into Ω_I and hence generates the action potential. In the computation, the finite element method is used for both the original system and the EN model. For the original system, an implicit scheme for nonlinear terms is adopted to avoid some stability issues due to small parameter ϵ, and the "exact" numerical solution is calculated with time step size $\Delta t = 10^{-4}$. For the EN model, there is no BL, and it allows for relatively larger time step sizes. We try three implementations for the EN model with different time step sizes $\Delta t = 10^{-4},\ 5 \times 10^{-3},\ 10^{-3}$. Figure 8 shows the dynamics of membrane potential $V_m(x, t) = \psi_I - \psi_E$ at different locations of a membrane obtained by using the original model and the EN model. The action potential first occurs at $x = 0$ and then propagates to the positive x. The error of V_m at $x = 1000$ is also shown in the figure, indicating good agreement of the two models. The computation time and the maximum error for V_m are listed in Table IV compared with the exact results for the original system. It indicates that it costs 56 h for the original system, while the computation time is greatly reduced with EN model, where all computations are done on the same computer (processor: 4 GHz, i76700K; memory: 32 GB). So the EN model is more efficient with acceptable accuracy. The conductance velocity is defined as the velocity that the action potential (the electric signal) travels along the axon. In this example, it is estimated as 1.3 m/s in dimensional quantities, which is the same order as usual estimates [35]. This is slightly larger than that in Ref. [35], since the length of an axon is not long enough and the boundary effect at $x = 0, 2000$ influences the velocity.

In the second case, we consider the myelinated axon, where conductances $G_{p_i}(x)$ are nonzero at only unmyelinated parts (typically the nodes). By Ref. [40], each segment between nodes is roughly 100–300 (scaled by 1 μm); here it is set to 200. To see the qualitative effect, we increase the portion of the myelinated part in each segment of the axon, where the portions 3/4 and 9/10 are tested. Figure 9 shows the propagation of the action potential for myelinated axon, calculated with the EN model. In the figures, blue and red curves represent the action potential at some locations for myelinated and unmyelinated parts, respectively. The action potential is initiated at the $x = 0$, weakens at myelinated parts, and reinforces a little at the unmyelinated part (node) of

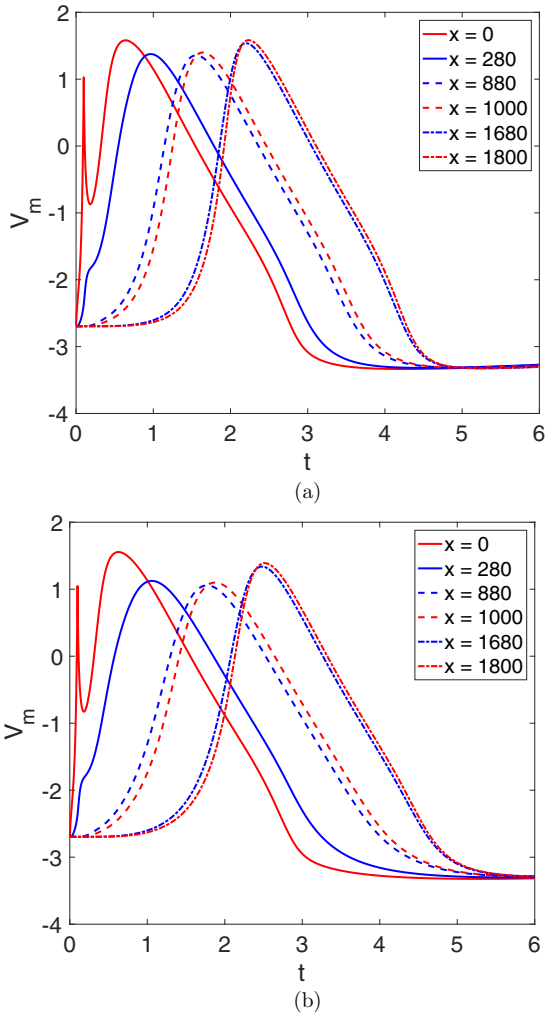

FIG. 9. Numerical results of propagation of action potential for myelinated axon: (a) 3/4 myelinated, (b) 9/10 myelinated.

each segment. For the 3/4 myelinated axon, the peak values of the action potential gradually decrease from about 1.6 at $x = 0$ to about 1.4 at $x = 1000$ and recover to about 1.6 at $x = 1800$. For the 9/10 myelinated axon, the peak values of action potential decrease from about 1.6 at $x = 0$ to about 1.1 at $x = 1000$ and then increase to about 1.4 at $x = 1800$. In the latter case, the tested axon is not long enough for the signal (action potential) to fully recover to its original strength.

V. CONCLUSIONS

In this work, we have investigated a multidimensional dynamic PNP system with various boundary conditions, and have derived the corresponding EN system with effective boundary conditions. In the case of Dirichlet boundary conditions, the effective conditions can be considered as a generalization of continuity of electrochemical potential. For flux conditions, we derived a physically correct effective conditions by keeping some essential high-order terms, which are important in many biological applications. The effective conditions for the general multi-ion species case involves elliptic integrals, and these extra terms of elliptic integrals account for the accumulation of ions in the BL and the spatial variation along the boundary. We have validated our EN models with several examples and demonstrated the effectiveness of the EN system with the implementation of the well-known Hodgkin-Huxley model for propagation of the action potential on an axon.

As a next step, for the biological example in Sec. IV we plan to analyze the reduction from the EN system to the classic cable model, under some consistent assumptions. We also plan to extend our approach to a modified PNP system where the size effect of the ions is included.

ACKNOWLEDGMENT

This work is in part supported by NSERC (CA) and the Fields Institute.

APPENDIX A: PROOFS IN SECTION II

Proof of Proposition 1. Under the assumptions of LEN and NGEN and from some previous steady-state analysis [1,41], we expect a BL with thickness $O(\epsilon)$ near $r = r_0$. In BL, we make the transformation

$$\Phi(R) = \psi(r), \quad N(R) = n(r),$$
$$P(R) = p(r), \quad R = \frac{r_0 - r}{\epsilon}, \tag{A1}$$

where all of the new functions Φ, P, N and their derivatives are assumed to be $O(1)$. In Eq. (A1) and hereafter, the arguments (θ, t) in functions will be omitted for brevity. With such scaling, the leading order system of equations in BL is

$$-\partial_{RR}\Phi = P - N,$$
$$\partial_R(\partial_R P + P\partial_R\Phi) = O(\epsilon), \tag{A2}$$
$$\partial_R(\partial_R N - N\partial_R\Phi) = O(\epsilon).$$

It is quite standard as in Ref. [2] to obtain the leading-order BL solutions:

$$\Phi(R) = \phi_0 + 2\ln\frac{1 - e^{-\sqrt{2c_0}R}\tanh\left(\frac{\phi_0-\psi_0}{4}\right)}{1 + e^{-\sqrt{2c_0}R}\tanh\left(\frac{\phi_0-\psi_0}{4}\right)} + O(\epsilon),$$
$$P(R) = c_0\left[\frac{1 + e^{-\sqrt{2c_0}R}\tanh\left(\frac{\phi_0-\psi_0}{4}\right)}{1 - e^{-\sqrt{2c_0}R}\tanh\left(\frac{\phi_0-\psi_0}{4}\right)}\right]^2 + O(\epsilon), \tag{A3}$$
$$N(R) = c_0\left[\frac{1 - e^{-\sqrt{2c_0}R}\tanh\left(\frac{\phi_0-\psi_0}{4}\right)}{1 + e^{-\sqrt{2c_0}R}\tanh\left(\frac{\phi_0-\psi_0}{4}\right)}\right]^2 + O(\epsilon),$$

where the constants c_0, ϕ_0, ψ_0 are functions of (θ, t). The composite solutions are given by

$$p(r) = P(R) + c(r) - c_0 + O(\epsilon),$$
$$n(r) = N(R) + c(r) - c_0 + O(\epsilon), \tag{A4}$$
$$\psi(r) = \Phi(R) + \phi(r) - \phi_0 + O(\epsilon),$$

which are uniformly valid in the domain Ω. Since in the bulk we have $p(r) = c(r) + O(\epsilon^2)$ by (6), it is reasonable to expect $p(r) = c(r) + o(\epsilon)$ in some intermediate region $r_0 - r \sim O(\epsilon^\alpha)$ with $0 < \alpha < 1$, say, $\alpha = 1/2$.

Next, we consider the $O(\epsilon)$ correction term, since we have kept such terms in Eqs. (7) for $c(r)$. We take cation $p(r)$, for example. The transport equation can be written as

$$\frac{\partial\left(rJ_p^r\right)}{\partial r} = -r\frac{\partial p}{\partial t} - \frac{\partial J_p^\theta}{\partial \theta}. \tag{A5}$$

In BL with $r = r_0 - \epsilon R$ and $\partial_r = -\frac{1}{\epsilon}\partial_R$, we have

$$J_p^r(R) = J_{p,0}^r(R) + O(\epsilon R), \tag{A6}$$

where $J_{p,0}^r$ is some unknown normal flux at the boundary $r = r_0$. Then, by definition of J_p^r and using the scale (A1), we get

$$\frac{\partial P}{\partial R} + P\frac{\partial \Phi}{\partial R} = \epsilon J_{p,0}^r + O(\epsilon^2 R). \tag{A7}$$

From Proposition 2, we see that $J_{p,0}^r \approx J_{c,0}^{r,+}$. Therefore, dividing by P and integrating, we obtain

$$\begin{aligned}&\ln(P(R)) + \Phi(R)\\ &\quad = \ln p_0 + \psi_0 + \epsilon J_{c,0}^{r,+}\int_0^R 1/P(z)\,dz + O(\epsilon^2 R),\end{aligned} \tag{A8}$$

where $P(R)$, $\Phi(R)$ on the left-hand side contain $O(\epsilon)$ terms, while for $P(z)$ inside the integral we can use the leading order solution (A3). By matching Ref. [42], let $R = \epsilon^{\alpha-1}s$ (i.e., $r_0 - r = \epsilon^\alpha s$) with $1/2 < \alpha < 1$, and we get

$$\begin{aligned}P(\epsilon^{\alpha-1}s) &= c(r_0 - \epsilon^\alpha s) + o(\epsilon),\\ \Phi(\epsilon^{\alpha-1}s) &= \phi(r_0 - \epsilon^\alpha s) + o(\epsilon).\end{aligned} \tag{A9}$$

Taking $R = \epsilon^{\alpha-1}s$ in the previous relation (A8), we get from left-hand side

$$\begin{aligned}&\ln(P(R)) + \Phi(R)\\ &\quad = \ln(c_0) + \phi_0 - \left[\frac{\partial_r c(r_0)}{c_0} + \partial_r\phi(r_0)\right]\epsilon^\alpha s + o(\epsilon),\end{aligned} \tag{A10}$$

and from the integral on the right-hand side

$$\epsilon\int_0^R 1/P(z)\,dz = \frac{\epsilon^\alpha s}{c_0} + \frac{\sqrt{2}\epsilon}{c_0^{3/2}}(e^{(\psi_0-\phi_0)/2} - 1) + o(\epsilon). \tag{A11}$$

In view of the definition $J_{c,0}^{r,+}$, the $\epsilon^\alpha s$ terms automatically cancel each other, then substituting into (A8) leads to $(11)_1$.

Proof of Proposition 2. We take cation $p(r)$ for an example. From equation $(5)_2$ of the PNP system, we easily get for some finite $\delta > 0$ (say, $\delta = r_0/2$)

$$(r_0 - \delta)J_p^r(r_0 - \delta) = r_0 J_{p,0}^r - \int_{r_0}^{r_0-\delta}\left(r\frac{\partial p}{\partial t} + \frac{\partial J_p^\theta}{\partial \theta}\right)dr. \tag{A12}$$

Similarly, from $(7)_1$ of the EN system, we obtain

$$(r_0 - \delta)J_c^{r,+}(r_0 - \delta) = r_0 J_{c,0}^{r,+} - \int_{r_0}^{r_0-\delta}\left(r\frac{\partial c}{\partial t} + \frac{\partial J_c^{\theta,+}}{\partial \theta}\right)dr. \tag{A13}$$

Based on assumptions (4) and (6), we get

$$J_c^{r,+}(r_0 - \delta) = J_p^r(r_0 - \delta) + O(\epsilon^2). \tag{A14}$$

Then immediately combining (A12)–(A14) gives

$$\begin{aligned}r_0 J_{c,0}^{r,+} = r_0 J_{p,0}^r &- \int_{r_0}^{r_0-\delta} r\frac{\partial(p-c)}{\partial t}\\ &+ \frac{\partial\left(J_p^\theta - J_c^{\theta,+}\right)}{\partial\theta}dr + O(\epsilon^2).\end{aligned} \tag{A15}$$

In the following, we shall simplify the integral in the above equation. For simplicity, we denote the zeta potential [43,44] as

$$\zeta(\theta, t) = \phi_0(\theta, t) - \psi_0(\theta, t). \tag{A16}$$

The first term in the integral of Eq. (A15) is calculated as

$$\begin{aligned}&\int_{r_0}^{r_0-\delta} r\frac{\partial(p-c)}{\partial t}\,dr\\ &\quad = \int_{r_0}^{r_0-\sqrt{\epsilon}} r\frac{\partial(p-c)}{\partial t}\,dr + o(\epsilon)\\ &\quad = \int_{r_0}^{r_0-\sqrt{\epsilon}} r_0\frac{\partial(p-c)}{\partial t}\,dr + o(\epsilon)\\ &\quad = -\epsilon\int_0^\infty r_0\frac{\partial(P-c_0)}{\partial t}\,dR + o(\epsilon)\\ &\quad = -\epsilon r_0\partial_t[\sqrt{2c_0}(e^{\zeta/2} - 1)] + o(\epsilon),\end{aligned} \tag{A17}$$

where we have used the assumption that $p = c + o(\epsilon)$ for $r_0 - r \geqslant \sqrt{\epsilon}$, and by setting the upper limit of integral as ∞ only exponentially small terms are neglected. For the second term in the integral of Eq. (A15), we first write

$$\begin{aligned}&J_p^\theta - J_c^{\theta,+}\\ &\quad = -\frac{1}{r}\left[\frac{\partial(p-c)}{\partial\theta} + p\frac{\partial\psi}{\partial\theta} - c\frac{\partial\phi}{\partial\theta}\right]\\ &\quad = -\frac{1}{r}\left[\frac{\partial(p-c)}{\partial\theta} + (p-c)\frac{\partial\phi}{\partial\theta} + p\frac{\partial(\psi-\phi)}{\partial\theta}\right].\end{aligned} \tag{A18}$$

Then, similarly to (A17), the integrals of first two parts in Eq. (A18) are readily found as

$$\begin{aligned}-\int_{r_0}^{r_0-\delta}\frac{1}{r}\frac{\partial(p-c)}{\partial\theta}\,dr &= \frac{\epsilon}{r_0}\partial_\theta[\sqrt{2c_0}(e^{\zeta/2} - 1)] + o(\epsilon),\\ -\int_{r_0}^{r_0-\delta}\frac{1}{r}(p-c)\frac{\partial\phi}{\partial\theta}\,dr &= \epsilon\frac{\sqrt{2c_0}}{r_0}(e^{\zeta/2} - 1)\frac{\partial\phi_0}{\partial\theta} + o(\epsilon).\end{aligned} \tag{A19}$$

For the third part in Eq. (A18), by using the explicit solutions (A3), we get

$$\begin{aligned}
&-\int_{r_0}^{r_0-\delta} \frac{p}{r}\frac{\partial(\psi-\phi)}{\partial\theta}\,dr \\
&= -\int_{r_0}^{r_0-\sqrt{\epsilon}} \frac{p}{r_0}\frac{\partial(\psi-\phi)}{\partial\theta}\,dr + o(\epsilon) \\
&= \frac{\epsilon}{r_0}\int_0^{\infty} P(R)\frac{\partial(\Phi-\phi_0)}{\partial\theta}\,dR + o(\epsilon) \\
&= -\frac{\epsilon}{r_0}\{\sqrt{2c_0}\partial_\theta(e^{\zeta/2}) - (e^{\zeta/2}-1)\partial_\theta(\sqrt{2c_0})\} + o(\epsilon).
\end{aligned} \tag{A20}$$

Combining above formulas in Eqs. (A18)–(A20), we obtain

$$\begin{aligned}
&\int_{r_0}^{r_0-\delta} \left(J_p^{\theta} - J_c^{\theta,+}\right) dr \\
&\quad = \frac{\epsilon}{r_0}(e^{\zeta/2}-1)[2\partial_\theta(\sqrt{2c_0}) + \sqrt{2c_0}\partial_\theta(\phi_0)] + o(\epsilon).
\end{aligned} \tag{A21}$$

Finally from (A15), (A17), and (A21), we obtain $(14)_1$.

Proof of Theorem 1. The proof follows similar lines as Proposition 2, and here we will mention the key different steps. For a domain inside and near Γ, we adopt the scalings

$$\Phi(X) = \psi(\xi), \quad P_i(X) = p_i(\xi), \quad X = -\frac{\xi}{\epsilon}, \tag{A22}$$

where $i = 1, \ldots, n$, and arguments (η, t) are omitted hereafter. In the multi-ion case, the previous explicit solutions in Eq. (A3) cannot be used anymore. Instead, by the BL analysis, we get

$$\begin{aligned}
-\partial_{XX}\Phi &= \sum_{i=1}^{n} z_i P_i(X) + O(\epsilon) \\
&= \sum_{i=1}^{n} z_i c_{i0} e^{z_i[\phi_0 - \Phi(X)]} + O(\epsilon).
\end{aligned} \tag{A23}$$

Integrating once gives

$$\partial_X\Phi = \pm\sqrt{2\sum_{i=1}^{n} c_{i0}(e^{z_i[\phi_0-\Phi(X)]}-1)} + O(\epsilon), \tag{A24}$$

where $\pm$ are chosen for the cases $\psi_0 \leqslant \phi_0$ and $\psi_0 \geqslant \phi_0$, respectively.

In the (ξ, η) coordinate system, in some region near boundary Γ, the normal and tangential fluxes for PNP system are given by

$$\begin{aligned}
J_{p_i}^{\xi} &= \mathbf{e}_\xi \cdot \mathbf{J}_{p_i} = -D_i\left(\frac{\partial p_i}{\partial\xi} + z_i p_i \frac{\partial\psi}{\partial\xi}\right), \\
J_{p_i}^{\eta} &= \mathbf{e}_\eta \cdot \mathbf{J}_{p_i} = -\frac{D_i}{\tilde{g}}\left(\frac{\partial p_i}{\partial\eta} + z_i p_i \frac{\partial\psi}{\partial\eta}\right),
\end{aligned} \tag{A25}$$

where

$$\tilde{g}(\eta, \xi) = [1 - \kappa(\eta)\xi]g(\eta). \tag{A26}$$

Similarly the fluxes $J_{c_i}^{\xi}$, $J_{c_i}^{\eta}$ for EN system can be defined by replacing p_i by c_i.

In terms of the fluxes (A25), the transport equation $(2)_2$ for p_i can be written as

$$-\frac{\partial p_i}{\partial t} = \frac{\partial J_{p_i}^{\xi}}{\partial\xi} - \frac{\kappa}{1-\kappa\xi}J_{p_i}^{\xi} + \frac{1}{\tilde{g}}\frac{\partial J_{p_i}^{\eta}}{\partial\eta}. \tag{A27}$$

Multiplying the factor $(1-\kappa\xi)$ on both sides and rearranging terms give

$$\frac{\partial}{\partial\xi}\left((1-\kappa\xi)J_{p_i}^{\xi}\right) = -(1-\kappa\xi)\frac{\partial p_i}{\partial t} - \frac{1}{g}\frac{\partial J_{p_i}^{\eta}}{\partial\eta}. \tag{A28}$$

Likewise, the transport equation (19) for c_i is

$$\frac{\partial}{\partial\xi}\left[(1-\kappa\xi)J_{c_i}^{\xi}\right] = -(1-\kappa\xi)\frac{\partial c_i}{\partial t} - \frac{1}{g}\frac{\partial J_{c_i}^{\eta}}{\partial\eta}. \tag{A29}$$

Integrating (A28) and (A29) from 0 to δ and using the fact $J_{c_i}^{\xi}(\delta) = J_{p_i}^{\xi}(\delta) + O(\epsilon^2)$ in the bulk, we obtain

$$\begin{aligned}
J_{c_i,0}^{\xi} = J_{p_i,0}^{\xi} - \int_0^{\delta}\left\{(1-\kappa\xi)\frac{\partial(p_i-c_i)}{\partial t} + \frac{1}{g}\frac{\partial(J_{p_i}^{\eta} - J_{c_i}^{\eta})}{\partial\eta}\right\}d\xi \\
+ O(\epsilon^2),
\end{aligned} \tag{A30}$$

where $\delta > 0$ is some typical bulk value.

Next, we shall simplify the integral in Eq. (A30), by using leading order relations in Eqs. (A23) and (A24). We get from the first term that

$$\begin{aligned}
&\int_0^{\delta}(1-\kappa\xi)\frac{\partial(p_i-c_i)}{\partial t}\,d\xi = -\epsilon\partial_t F_{i0} + o(\epsilon), \\
&F_{i0} = \int_0^{\infty}[P_i(X) - c_{i0}]dX \\
&\quad = \pm\frac{c_{i0}}{\sqrt{2}}\int_1^{e^{\phi_0-\psi_0}} \frac{u^{z_i}-1}{\sqrt{\sum_{k=1}^{n} c_{k0}(u^{z_k}-1)}}\frac{du}{u},
\end{aligned} \tag{A31}$$

where we have made use of the assumption that κ is $O(1)$ [or at least $\kappa < O(1/\epsilon)$]. We have used (A23) and (A24) in F_{i0}, and the remaining terms have been put to the $o(\epsilon)$ term. For the second term in integral of (A30), we write the flux difference as

$$\begin{aligned}
&J_{p_i}^{\eta} - J_{c_i}^{\eta} \\
&\quad = -\frac{D_i}{\tilde{g}}\left[\frac{\partial(p_i-c_i)}{\partial\eta} + z_i(p_i-c_i)\frac{\partial\phi}{\partial\eta} + z_i p_i\frac{\partial(\psi-\phi)}{\partial\eta}\right],
\end{aligned} \tag{A32}$$

and integration leads to

$$\begin{aligned}
\int_0^{\delta}\left(J_{p_i}^{\eta} - J_{c_i}^{\eta}\right)d\xi = \frac{D_i}{g}\Bigg[\epsilon\partial_\eta F_{i0} + \epsilon z_i F_i\partial_\eta\phi_0 \\
+ \int_0^{\delta} z_i p_i\frac{\partial(\psi-\phi)}{\partial\eta}\,d\xi\Bigg] + o(\epsilon),
\end{aligned} \tag{A33}$$

where the last term is given by

$$\begin{aligned}
&\int_0^\delta z_i p_i \frac{\partial(\psi-\phi)}{\partial\eta}\,d\xi \\
&= -\epsilon\int_0^\infty z_i P_i(X)\frac{\partial(\Phi-\phi_0)}{\partial\eta}\,dX + o(\epsilon) \\
&= -\epsilon c_{i0}\int_0^\infty z_i e^{z_i(\phi_0-\Phi)}\frac{\partial(\Phi-\phi_0)}{\partial\eta}\,dX + o(\epsilon) \\
&= \epsilon c_{i0}\partial_\eta\int_0^\infty (e^{z_i(\phi_0-\Phi)}-1)\,dX + o(\epsilon) \\
&= \epsilon c_{i0}\partial_\eta\left(\frac{1}{c_{i0}}F_{i0}\right) + o(\epsilon). \qquad \text{(A34)}
\end{aligned}$$

Finally, combining Eqs. (A30), (A31), (A33), and (A34) gives the result in (22). It can be shown as in Appendix A of Ref. [2] that the function F_i is well defined near $\phi_0 = \psi_0$.

Proof of Theorem 1 in three dimensions. In the 3D case, local coordinates (ξ, η_1, η_2) will be adopted, where η_1, η_2 are parameters of surface Γ along two principal directions $\mathbf{e}_1, \mathbf{e}_2$. The surface Γ is characterized by metric g_1, g_2 and curvatures κ_1, κ_2. Then the flux of PNP system is written as

$$\mathbf{J}_{p_i} = J^\xi_{p_i}\mathbf{e}_\xi + \mathbf{J}^\Gamma_{p_i} = J^\xi_{p_i}\mathbf{e}_\xi + J^{\eta_1}_{p_i}\mathbf{e}_1 + J^{\eta_2}_{p_i}\mathbf{e}_2, \qquad \text{(A35)}$$

and the explicit expressions for the components will be similar to (A25) and (A26). The counterpart of (A27) is

$$\begin{aligned}
-\frac{\partial p_i}{\partial t} &= \frac{\partial J^\xi_{p_i}}{\partial\xi} - \left(\frac{\kappa_1}{1-\kappa_1\xi}+\frac{\kappa_2}{1-\kappa_2\xi}\right)J^\xi_{p_i} \\
&\quad + [1+O(\kappa\xi)]\nabla_\Gamma\cdot\mathbf{J}^\Gamma_{p_i}, \qquad \text{(A36)}
\end{aligned}$$

where $\kappa = \max\{|\kappa_1|, |\kappa_2|\}$. Rearranging terms gives

$$\begin{aligned}
&\frac{\partial}{\partial\xi}\left[(1-\kappa_1\xi)(1-\kappa_2\xi)J^\xi_{p_i}\right] \\
&\quad = -[1+O(\kappa\xi)]\left(\frac{\partial p_i}{\partial t} + \nabla_\Gamma\cdot\mathbf{J}^\Gamma_{p_i}\right). \qquad \text{(A37)}
\end{aligned}$$

Then we get [similar to (A30)]

$$J^\xi_{c_i,0} = J^\xi_{p_i,0} - \int_0^\delta\left\{\frac{\partial(p_i-c_i)}{\partial t} + \nabla_\Gamma\cdot\left(\mathbf{J}^\Gamma_{p_i}-\mathbf{J}^\Gamma_{c_i}\right)\right\}d\xi, \qquad \text{(A38)}$$

where $o(\epsilon)$ terms are omitted. The later proof will be straightforward as 2D by referring to the identity in the BL:

$$\begin{aligned}
\mathbf{J}^\Gamma_{p_i} - \mathbf{J}^\Gamma_{c_i} &= -[1+O(\kappa\epsilon)]D_i[\nabla_\Gamma(p_i-c_i) \\
&\quad + z_i(p_i-c_i)\nabla_\Gamma\phi + z_i p_i\nabla_\Gamma(\psi-\phi)]. \qquad \text{(A39)}
\end{aligned}$$

Proof of Theorem 2. The proof follows similar lines as Proposition 1. We only need to start with Eq. (A28) instead of Eq. (A5). Then with the scale $X = -\xi/\epsilon$, we get

$$J^\xi_{p_i}(X) = J^\xi_{p_i,0}(X) + O(\epsilon X). \qquad \text{(A40)}$$

Then, similarly to (A8), one can get

$$\begin{aligned}
&\ln(P_i(X)) + z_i\Phi(X) \\
&\quad = \ln p_{i0} + z_i\psi_{i0} + \frac{\epsilon J^\xi_{c_i,0}}{D_i}\int_0^X 1/P_i(z)\,dz + O(\epsilon^2 X). \qquad \text{(A41)}
\end{aligned}$$

Finally by matching with $X\to\infty$, we get condition (25), and the term f_{i0} in Eq. (26) is defined from the above integral by using relations (A23) and (A24).

Proof of Theorem 3. In this case, $\psi(0,\eta,t)$ is not known, and so we need an additional condition to determine $\psi_0 \equiv \psi(0,\eta,t)$ in flux conditions (22) and (23). From the relation (A24) and with $\partial_X = -\epsilon\partial_\xi$, we get at the leading order

$$-\epsilon\partial_\xi\psi(0) = \pm\sqrt{2\sum_{i=1}^n c_{i0}(e^{z_i(\phi_0-\psi_0)}-1)}, \qquad \text{(A42)}$$

where $\pm$ are chosen for the cases $\psi_0 \leqslant \phi_0$ and $\psi_0 \geqslant \phi_0$, respectively. Combining with $(28)_1$ leads to the nonlinear condition (29).

In the above, we have tacitly assumed that $\gamma \leqslant O(\epsilon)$, so that the remainder is $o(1)$ in Eq. (29). For the case $O(\epsilon) < \gamma \leqslant O(1)$, with the NGEN assumption in this work, some previous results [2,41] and numerical evidence in Sec. IV show that $\psi_i - \phi_i = o(1)$, which is consistent with (29). In fact, in BL we have

$$\begin{aligned}
\psi-\phi_0,\ p_i - c_{i0} &= O(\epsilon/\gamma), \\
\partial_\xi\psi,\ \partial_\xi p_i &= O(1/\gamma), \qquad \text{(A43)} \\
\partial_{\xi\xi}\psi &= O(1/(\gamma\epsilon)),\ldots.
\end{aligned}$$

So with slight modification of the transformation (e.g., $\Phi = \psi - \phi_0$), one can show that the relation (29) still holds at leading order.

APPENDIX B: FUNCTIONS IN THEOREMS 1, 2, AND 3

For some special cases, the explicit expressions for F_i, f_i and relation (29) are available. For $z_1 = 1, z_2 = -1$ in Theorem 1, we recover the result

$$\begin{aligned}
F_1(c_{10},\phi_0-\psi_0) &= \sqrt{2c_{10}}(e^{(\phi_0-\psi_0)/2}-1), \\
F_2(c_{10},\phi_0-\psi_0) &= \sqrt{2c_{10}}(e^{(\psi_0-\phi_0)/2}-1). \qquad \text{(B1)}
\end{aligned}$$

For the case $z_1 = 2, z_2 = -1$, we get

$$\begin{aligned}
F_1(c_{10},\phi_0-\psi_0) &= \sqrt{\frac{c_{10}}{2}}\left[e^{\frac{\phi_0-\psi_0}{2}}\sqrt{e^{(\phi_0-\psi_0)}+2}-\sqrt{3}\right], \\
F_2(c_{10},\phi_0-\psi_0) &= \sqrt{2c_{10}}(\sqrt{1+2e^{(\psi_0-\phi_0)}}-\sqrt{3}). \qquad \text{(B2)}
\end{aligned}$$

For the three-ion case with $z_1 = 1, z_2 = 1, z_3 = -1$, we have

$$\begin{aligned}
F_j(c_{10},c_{20},\phi_0-\psi_0) &= \sqrt{\frac{c_{j0}}{c_{10}+c_{20}}}\sqrt{2c_{j0}}\left(e^{\frac{\phi_0-\psi_0}{2}}-1\right), \\
F_3(c_{10},c_{20},\phi_0-\psi_0) &= \sqrt{2(c_{10}+c_{20})}(e^{(\psi_0-\phi_0)/2}-1), \qquad \text{(B3)}
\end{aligned}$$

where $j = 1, 2$.

For the case $z_1 = 1, z_2 = -1$ in Theorem 2, we have

$$f_1(c_{10}, \phi_0 - \psi_0) = \frac{\sqrt{2}(e^{(\psi_0-\phi_0)/2} - 1)}{c_{10}^{3/2}},$$
$$f_2(c_{10}, \phi_0 - \psi_0) = \frac{\sqrt{2}(e^{(\phi_0-\psi_0)/2} - 1)}{c_{10}^{3/2}}. \quad \text{(B4)}$$

For the case $z_1 = 2, z_2 = -1$, we get

$$f_1 = \frac{\sqrt{2 + e^{\phi_0-\psi_0}}(1 + 2e^{\phi_0-\psi_0})e^{\frac{3}{2}(\psi_0-\phi_0)} - 3\sqrt{3}}{3\sqrt{2}c_{10}^{3/2}},$$
$$f_2 = \frac{\operatorname{arcsinh}(e^{(\phi_0-\psi_0)/2}/\sqrt{2}) - \operatorname{arccsch}(\sqrt{2})}{\sqrt{2}c_{10}^{3/2}}. \quad \text{(B5)}$$

For the case with $z_1 = 1, z_2 = 1, z_3 = -1$, we have

$$f_j(c_{10}, c_{20}, \phi_0 - \psi_0) = \frac{\sqrt{2}(e^{(\psi_0-\phi_0)/2} - 1)}{c_{j0}\sqrt{c_{10} + c_{20}}},$$
$$f_3(c_{10}, c_{20}, \phi_0 - \psi_0) = \frac{\sqrt{2}(e^{(\phi_0-\psi_0)/2} - 1)}{(c_{10} + c_{20})^{3/2}}, \quad \text{(B6)}$$

where $j = 1, 2$.

In Theorem 3, for the case $z_1 = 1, z_2 = -1$, the relation (29) becomes

$$\psi_0 - \tilde{\psi}_0 = \frac{\gamma}{\epsilon}\sqrt{2c_{10}}(e^{(\phi_0-\psi_0)/2} - e^{(\psi_0-\phi_0)/2}). \quad \text{(B7)}$$

For the case $z_1 = 1, z_2 = 1, z_3 = -1$, it becomes

$$\psi_0 - \tilde{\psi}_0 = \frac{\gamma}{\epsilon}\sqrt{2c_{30}}(e^{(\phi_0-\psi_0)/2} - e^{(\psi_0-\phi_0)/2}), \quad \text{(B8)}$$

where $c_{30} = c_{10} + c_{20}$ by EN condition.

APPENDIX C: THE DATA USED IN SECTION IV

The data are mainly from papers [27,35] and the book [39]. The temperature in Ref. [27] is set to be 6.3 °C, so we get $T = 279.45$ K. The other constants are

$$k_B = 1.38 \times 10^{-23}\ \text{J/K}, \quad N_A = 6.022 \times 10^{23}/\text{mol},$$
$$e_0 = 1.602 \times 10^{-19}\ \text{C}, \quad \epsilon_0 = 8.854 \times 10^{-12}\ \text{C/(V} \cdot \text{m)}. \quad \text{(C1)}$$

The typical bulk concentrations for Na^+, K^+, Cl^- are

	p_1, Na^+	p_2, K^+	p_3, Cl^-
Extracellular	100 mM	4 mM	104 mM
Intracellular	12 mM	125 mM	137 mM

which are used as initial conditions (scaled by p_0 below). Some typical values are (diffusivity of Cl^- is from Ref. [45])

$$\epsilon_r = 80, \quad \epsilon_r^m = 2, \quad h_m = 5\ \text{nm},$$
$$L_1 = 100\ \mu\text{m–10 mm}, \quad L_2 = 1\ \mu\text{m},$$
$$p_0 = 100\ \text{mM} = 100\ \text{mol/m}^3, \quad \text{(C2)}$$
$$D_0 = 10^{-5}\ \text{cm}^2/\text{s} = 10^{-9}\ \text{m}^2/\text{s},$$
$$D_1 = 1.33D_0,\ D_2 = 1.96D_0,\ D_3 = 2.03D_0.$$

The conductances are given by

$$\bar{G}_{\text{Na}} = 120\ \text{mS/cm}^2 = 1200\ \text{C/(V} \cdot \text{s} \cdot \text{m}^2),$$
$$\bar{G}_{\text{K}} = 360\ \text{C/(V} \cdot \text{s} \cdot \text{m}^2),$$
$$\bar{G}_{\text{Na,leak}} = 1.04\ \text{C/(V} \cdot \text{s} \cdot \text{m}^2),$$
$$\bar{G}_{\text{K,leak}} = 4\ \text{C/(V} \cdot \text{s} \cdot \text{m}^2). \quad \text{(C3)}$$

where leak conductances are set to ensure that resting potential is roughly 65 mV.

From the above data, we get

$$\frac{k_B T}{e_0} \approx 24\ \text{mV}, \quad \frac{L_2^2}{D_0} = 1\ \text{ms},$$
$$G_0 = \frac{p_0 D_0 e^2 N_A}{k_B T L_2} \approx 400\,758\ \text{C/(V} \cdot \text{s} \cdot \text{m}^2). \quad \text{(C4)}$$

For the dimensionless system we have (the tilde is removed)

$$\epsilon = 1.33 \times 10^{-3}, \quad \epsilon_m = 2.1 \times 10^{-4},$$
$$h_m = 5 \times 10^{-3}, \quad L_1 = 100 \sim 10^4,$$
$$D_1 = 1.33, \quad D_2 = 1.96, \quad D_3 = 2.03, \quad \text{(C5)}$$
$$\bar{G}_{\text{Na}} = 3 \times 10^{-3}, \quad \bar{G}_{\text{K}} = 9 \times 10^{-4},$$
$$\bar{G}_{\text{Na,leak}} = 2.6 \times 10^{-6}, \quad \bar{G}_{\text{K,leak}} = 1 \times 10^{-5}.$$

APPENDIX D: NONDIMENSIONALIZATION AND DYNAMIC SYSTEM FOR m, h, and n

First, the dimensional PNP system is given by (1) with $n = 3$ and $z_1 = z_2 = 1, z_3 = -1$, in domain $\Omega = [0, L_1] \times [0, L_2]$. Here we have assumed the same ϵ_r for extracellular and intracellular regions. The dimensional relation for the current through the membrane or ion channel, from the intracellular region to extracellular region, is

$$I_i = G_{p_i}(x)(V_m - E_i), \quad i = 1, 2, 3, \quad \text{(D1)}$$

or in terms of normal flux at $y = L_2/2$

$$z_i e_0 N_A J_{p_i}^y \equiv -z_i e_0 N_A D_i \left(\partial_y p_i + \frac{e_0}{k_B T} z_i p_i \partial_y \psi\right)$$
$$= G_{p_i}\left(\psi_I - \psi_E - \frac{k_B T}{z_i e_0} \ln \frac{p_{iE}}{p_{iI}}\right), \quad \text{(D2)}$$

where G_{p_i} is the conductance [cf. (44)] for ion p_i, E_i is the Nernst potential of ion p_i, and $V_m = \psi_I - \psi_E$ is the membrane potential. Hereafter, subscripts I and E denote the values or limit values at the membrane $y = L_2/2$ from the intracellular and extracellular regions, respectively.

Suppose the membrane has a small thickness h_m and a relative permittivity ϵ_r^m, and assume there are no ions in membrane. Thus, the electric potential is linear (a constant electric field) inside the membrane. The interface conditions for ψ on the membrane $y = L_2/2$ are

$$\epsilon_r \partial_y \psi|_{y=\frac{L_2}{2}\pm} = \epsilon_r^m \frac{\psi_E - \psi_I}{h_m}, \quad \text{(D3)}$$

where $\frac{L_2}{2}\pm$ mean limits at the membrane from upper and lower regions.

For nondimensionalization, we adopt the following scalings:

$$\tilde{\psi} = \frac{\psi}{k_B T/e_0}, \quad \tilde{p}_i = \frac{p_i}{p_0}, \quad \tilde{L}_1 = \frac{L_1}{L_2}, \quad \tilde{x} = \frac{x}{L_2}, \quad \tilde{y} = \frac{y}{L_2}, \quad \tilde{h}_m = \frac{h_m}{L_2}, \quad \tilde{D}_i = \frac{D_i}{D_0}, \quad \tilde{t} = \frac{t}{L_2^2/D_0}, \quad \tilde{G}_{p_i} = \frac{G_{p_i}}{G_0}, \tag{D4}$$

where the length scale L_2 is adopted as in Ref. [2] so that it gives the correct timescale for the action potential, p_0 is the typical concentration of ions, D_0 is the typical diffusion constant, and typical conductance G_0 is defined by $G_0 = p_0 D_0 e^2 N_A/(k_B T L_2)$. All the parameter values and typical values are given in Appendix C. Substituting into (1) and removing the tilde lead to the system (2) with $n = 3$ in Sec. IV A. The interface conditions are treated similarly, and we obtain (43) with the tilde removed in $\tilde{G}_{p_i}$ and (45) with the dimensionless capacitance

$$C_m = \frac{\epsilon_m^2}{\tilde{h}_m}. \tag{D5}$$

In this system, the dimensionless parameters ϵ and ϵ_m are defined by

$$\epsilon = \sqrt{\frac{\epsilon_0 \epsilon_r k_B T}{e_0^2 N_A p_0 L_2^2}}, \quad \epsilon_m = \sqrt{\frac{\epsilon_0 \epsilon_r^m k_B T}{e_0^2 N_A p_0 L_2^2}}. \tag{D6}$$

The dynamics for m, h, n in Eq. (44) are given by [39]

$$\frac{dn}{dt} = \alpha_n(1-n) - \beta_n n, \quad \frac{dm}{dt} = \alpha_m(1-m) - \beta_m m, \quad \frac{dh}{dt} = \alpha_h(1-h) - \beta_h h. \tag{D7}$$

The coefficients depend on V_m and are given by

$$\alpha_n = \frac{1}{100}\frac{10-\bar{V}}{(e^{(10-\bar{V})/10}-1)}, \quad \beta_n = \frac{1}{8e^{\bar{V}/80}}, \quad \alpha_m = \frac{1}{10}\frac{25-\bar{V}}{(e^{(25-\bar{V})/10}-1)},$$
$$\beta_m = 4e^{-\bar{V}/18}, \quad \alpha_h = \frac{7}{100}e^{-\bar{V}/20}, \quad \beta_h = \frac{1}{e^{(30-\bar{V})/10}+1}, \tag{D8}$$

where $\bar{V} = V_m - V_r$ and V_r is some fixed resting potential. In above coefficients, the unit for $\bar{V}$ is millivolts. Theoretically, there is no singularity in the above coefficients, but for computation special treatment is performed as Ref. [2] when $\bar{V}$ is near 10 or 25. With $\bar{V} = 0$, we obtain the steady-state solution:

$$n_\infty \approx 0.3177, \quad m_\infty \approx 0.05293, \quad h_\infty \approx 0.5961, \tag{D9}$$

which are used to generate the resting state and used as initial values of the time-dependent problem to simulatethe action potential. For the dimensionless system in Sec. IV A, we still use the system (D7) and will not scale the quantities in the coefficients (D8), where the quantity $\bar{V}$ (in millivolts) is related to the normalized membrane potential $V_m = \psi_I - \psi_E$ through

$$\bar{V} = \frac{k_B T}{e_0}(\psi_I - \psi_E) - V_r, \tag{D10}$$

and $V_r = -65$ mV is the resting potential in millivolts [see (59)].

[1] I. Rubinstein, *Electro-diffusion of Ions* (SIAM, Philadelphia, PA, 1990).
[2] Z. Song, X. Cao, and H. Huang, Phys. Rev. E **97**, 012411 (2018).
[3] D. Gillespie and R. S. Eisenberg, Phys. Rev. E **63**, 061902 (2001).
[4] T.-L. Horng, T.-C. Lin, C. Liu, and B. Eisenberg, J. Phys. Chem. B **116**, 11422 (2012).
[5] P. A. Markowich, *The Stationary Semiconductor Device Equations* (Springer Science & Business Media, Berlin, 2013).
[6] J. J. Jasielec, G. Lisak, M. Wagner, T. Sokalski, and A. Lewenstam, Electroanalysis **25**, 133 (2013).
[7] A. Singer, D. Gillespie, J. Norbury, and R. Eisenberg, Eur. J. Appl. Math. **19**, 541 (2008).
[8] A. Singer and J. Norbury, SIAM J. Appl. Math. **70**, 949 (2009).
[9] W. Liu, J. Diff. Equ. **246**, 428 (2009).
[10] W. Liu and H. Xu, J. Diff. Equ. **258**, 1192 (2015).
[11] G. Lin, W. Liu, Y. Yi, and M. Zhang, SIAM J. Appl. Dyn. Sys. **12**, 1613 (2013).
[12] B. Eisenberg, W. Liu, and H. Xu, Nonlinearity **28**, 103 (2015).
[13] X.-S. Wang, D. He, J. J. Wylie, and H. Huang, Phys. Rev. E **89**, 022722 (2014).
[14] I. Rubinstein, SIAM J. Appl. Math. **47**, 1076 (1987).
[15] H. Huang, J. J. Wylie, and R. M. Miura, Bull. Math. Biol. **73**, 1682 (2011).
[16] R. T. Mathias, Biophys. J. **48**, 435 (1985).
[17] E. Vaghefi, N. Liu, and P. J. Donaldson, Biomed. Eng. Online **12**, 85 (2013).
[18] H. Gao and D. He, J. Sci. Comput. **72**, 1269 (2017).

[19] A. Flavell, M. Machen, B. Eisenberg, J. Kabre, C. Liu, and X. Li, J. Comput. Electron. **13**, 235 (2014).
[20] C. Chainais-Hillairet, J.-G. Liu, and Y.-J. Peng, ESAIM: Math. Model. Numer. Anal. **37**, 319 (2003).
[21] C. Chainais-Hillairet and Y.-J. Peng, IMA J. Numer. Anal. **23**, 81 (2003).
[22] X. Cao and H. Huang (to be published).
[23] B. Lu, M. J. Holst, J. A. McCammon, and Y. Zhou, J. Comput. Phys. **229**, 6979 (2010).
[24] M. Mirzadeh and F. Gibou, J. Comput. Phys. **274**, 633 (2014).
[25] C. J. Budd, W. Huang, and R. D. Russell, SIAM J. Sci. Comput. **17**, 305 (1996).
[26] H. Tang and T. Tang, SIAM J. Numer. Anal. **41**, 487 (2003).
[27] A. Hodgkin and A. Huxley, Bull. Math. Biol. **52**, 25 (1990).
[28] B. Hille *et al.*, *Ion Channels of Excitable Membranes*, Vol. 507 (Sinauer, Sunderland, MA, 2001).
[29] H.-C. Chang and G. Jaffé, J. Chem. Phys. **20**, 1071 (1952).
[30] I. Lelidis, J. R. Macdonald, and G. Barbero, J. Phys. D **49**, 025503 (2015).
[31] Y. Mori, A three-dimensional model of cellular electrical activity, Ph.D. thesis, New York University, Graduate School of Arts and Science (2006).
[32] Y. Mori, Phys. D **308**, 94 (2015).
[33] A. L. Hodgkin and A. F. Huxley, J. Physiol. **117**, 500 (1952).
[34] J. Cooley and F. Dodge Jr., Biophys. J. **6**, 583 (1966).
[35] J. Pods, J. Schönke, and P. Bastian, Biophys. J. **105**, 242 (2013).
[36] N. Qian and T. Sejnowski, Biol. Cybern. **62**, 1 (1989).
[37] M. Léonetti, Eur. Phys. J. B **2**, 325 (1998).
[38] Y. Mori, arXiv:0901.3914.
[39] J. Malmivuo and R. Plonsey, *Bioelectromagnetism: Principles and Applications of Bioelectric and Biomagnetic Fields* (Oxford University Press, New York, 1995).
[40] M. C. Ford, O. Alexandrova, L. Cossell, A. Stange-Marten, J. Sinclair, C. Kopp-Scheinpflug, M. Pecka, D. Attwell, and B. Grothe, Nat. Commun. **6**, 8073 (2015).
[41] C.-C. Lee, H. Lee, Y. Hyon, T.-C. Lin, and C. Liu, Nonlinearity **24**, 431 (2010).
[42] A. W. Bush, *Perturbation Methods for Engineers and Scientists* (CRC Press, Boca Raton, FL, 1992).
[43] E. R. Cohen, *Quantities, Units and Symbols in Physical Chemistry* (Royal Society of Chemistry, Research Triangle Park, NC, 2007).
[44] B. J. Kirby, *Micro- and Nanoscale Fluid Mechanics: Transport in Microfluidic Devices* (Cambridge University Press, Cambridge, 2010).
[45] J.-L. Liu and B. Eisenberg, J. Chem. Phys. **141**, 22D532 (2014).